

1        **Investigation of DNA interaction and antiproliferative activity of mixed**  
2        **ligand dioxidomolybdenum(VI) complexes incorporating ONO donor**  
3        **aroylhydrazone ligands**

4        Rupam Dinda<sup>\*,a</sup>, Arpita Panda,<sup>a</sup> Atanu Banerjee,<sup>a</sup> Monalisa Mohanty,<sup>a</sup> Sagarika Pasayat,<sup>a</sup>  
5        Edward. R. T. Tiekink<sup>b</sup>

6        <sup>a</sup>Department of Chemistry, National Institute of Technology, Rourkela, 769008 Odisha,  
7        India.

8        <sup>b</sup>Research Centre for Crystalline Materials, School of Science and Technology, 5 Jalan  
9        Universiti, Sunway University, Bandar Sunway, Selangor Darul Ehsan 47500, Malaysia

10

11

12

13

14

15

16

17

18

19

20

---

21        \*Corresponding Author

22        E-mail: rupamdinda@nitrkl.ac.in (R. Dinda)

23        Tel.: + (91) 661 246 2657; Fax: + (91) 661 246 2022

24        **ORCID** ID: 0000-0001-9452-7791

1 **Abstract**

2 Four new mixed ligand dioxidomolybdenum(VI)  $[\text{Mo}^{\text{VI}}\text{O}_2\text{L}^{1-3}(\text{Q})]$  (**1–3**),  $[\text{Mo}^{\text{VI}}\text{O}_2\text{L}^4(\text{Q})]_2$   
3  $(\text{H}_2\text{O})$  (**4**) [where Q = MeOH for **1** and imidazole for **2–4**] complexes have been synthesized  
4 using four different ONO donor aroylhydrazone ligands ( $\text{H}_2\text{L}^{1-4}$ ). All the derived ligands and  
5 complexes were characterised by IR, UV-Vis, NMR spectroscopy and CHNS-analysis while  
6 the redox properties of the complexes have been investigated by cyclic voltammetry. The  
7 molecular geometries of **1–4** were established by X-ray crystallography and are closely related  
8 to each other, having a cis-Mo(=O)<sub>2</sub> core, a di-negative tridentate Schiff base ligand, which  
9 coordinates via the phenoxide-O1, amide-O4 and imine-N1 atoms, and with the sixth site  
10 occupied by an O-bound methanol molecule (**1**) or an N-bound imidazole molecule (**2–4**); **4**  
11 was isolated as a hydrate. The resultant NO<sub>5</sub> (**1**) and cis-N<sub>2</sub>O<sub>4</sub> (**2–4**) donor sets are each based  
12 on a distorted octahedron. The complexes have been explored for their interaction with CT-  
13 DNA, where moderate binding constants were observed in the range 10<sup>3</sup> to 10<sup>4</sup> M<sup>-1</sup>. The  
14 complexes showed different binding modes towards DNA such as intercalation, minor and  
15 major groove binding. Further, *in vitro* cytotoxicity activity of all the complexes were  
16 determined against HT-29 (colon cancer) and HeLa (cervical cancer) cell lines. Complex **4**,  
17 due to the presence of a heterocyclic 2-hydroxy-1-naphthyl moiety in the ligand backbone, was  
18 found to be comparatively more potent than the other complexes.

---

19 **Keywords:** Aroylhydrazone / Mixed ligand dioxidomolybdenum(VI) complexes / DNA  
20 binding/ Antiproliferative activity.

21

22

23

## 1 **Introduction**

2 Molybdenum is one of the major trace elements found in daily diet and is also found in three  
3 different enzymes present in humans namely, sulfite oxidase, xanthine oxidase and aldehyde  
4 oxidase that have functions in detoxification [1-4]. It has been reported that the lack of the  
5 required amount of molybdenum can increase the risk of esophageal cancer [5]. Studies showed  
6 cell-growth inhibition properties of various polyoxidomolybdates on some specific carcinoma  
7 cells, among which Mo(II) complexes produce good cytotoxicity results. Though there are few  
8 reports on molybdenum complexes as anticancer agents [6,7], it has been found that with  
9 increased chelation in the structure there is a decrease in anticancer properties [8].  
10 Molybdenum can also be considered a better replacement for cisplatin compared to other  
11 transition metals, due its labile nature and comparatively low cytotoxicity against non-  
12 cancerous cells [9].

13 Molybdenum complexes of Schiff base ligands have gained significant interest owing to their  
14 low-cost and ease of preparation. Further, ligand preparation is basically facile: reacting  
15 sterically and electronically varied amines and aldehydes, respectively, through aldol  
16 condensation [10-20]. Schiff base ligands also have the potential to stabilize various metal ions  
17 in different oxidation states [21-25]. Moreover, the presence of a rigid, aromatic backbone  
18 provides specific spectroscopic properties that make transition metal complexes potential  
19 probes for nucleic acids. These metal complexes form intermediates in many enzymatic  
20 reactions that include the reaction of enzymes with amino or carbonyl group of the complex  
21 [26-40].

22 Aryl hydrazones form a class of Schiff base organic scaffolds which show a wide range of  
23 biological properties including anticonvulsant and antituberculosis properties along with others  
24 like antibacterial, antifungal, antiinflammatory, antinociceptive and antiplatelet activities [41-  
25 43]. Recently, Iproniazide, a hydrazone derived drug, has been used in the treatment of

1 tuberculosis [44]. Also, an oral nitrofuran antibiotic named Nifuroxazide is used for the  
2 treatment of anti-dehydration and for the treatment of colitis [45]. Furazolidone is a synthetic  
3 nitrofuran derivative that is well known for its antileishmanial activity and also clinically used  
4 as an antiprotozoal and antibacterial agent [46-50]. The advantageous electronic properties of  
5 arylhydrazones also give rise to complexes with more effective DNA-binding and DNA  
6 cleavage activities [27,32,34,35,37]. Molybdenum complexes of Schiff bases of aryl  
7 hydrazones are attractive due to their various applications including catalysis [51], luminescent  
8 probes [52], molecular sensors [53] and also display impressive biological activities [54-58]  
9 owing to the presence of the metal centre. On the other hand, as substituted imidazoles are  
10 found to have antiprotozoal, antifungal and antihypertensive properties [59-61], it has been  
11 employed as a co-ligand in the present study, in order to increase the overall biological potential  
12 of the synthesized complexes.

13 In the past few years, our research group has investigated the synthesis of several transition  
14 metal complexes incorporating –ONO and –ONS donor ligand systems in order to explore  
15 their biological activity [24, 62-77]. In continuation of this work, herein we report four novel  
16 dioxidomolybdenum(VI) complexes with –ONO donor, aroylazine ligand systems ( $H_2L^{1-4}$ ).  
17 All the complexes are characterized by various spectroscopic methods and their structural  
18 features have been elucidated by X-ray crystallography. Furthermore, the complexes have been  
19 evaluated for their DNA interaction activity which shows a moderate binding affinity. Finally,  
20 the *in vitro* antiproliferative activities of **1–4** were assayed against the HT-29 (colon cancer)  
21 and HeLa (cervical cancer) cell lines and the mechanism of cell death for **4** ascertained by  
22 DAPI staining, i.e. apoptosis.

23

24

25

## 1 **Experimental Section**

### 2 **Materials and Methods**

3 The chemicals used herein were purchased from commercial sources, while the solvents were  
4 distilled under a dry nitrogen atmosphere according to the standard literature procedures [78,  
5 79] prior to use.  $[\text{MoO}_2(\text{acac})_2]$  was used as the metal precursor and synthesized as per the  
6 reported procedure [79]. Elemental analysis (CHNS) measurements were carried out in a Vario  
7 EL cube elemental analyser instrument. FT-IR spectra were recorded by employing a Perkin  
8 Elmer Spectrum RX I spectrophotometer. Electronic spectra were recorded on a PerkinElmer  
9 Lambda 25 spectrophotometer.  $^1\text{H}$  and  $^{13}\text{C}$  NMR spectra were measured on a 400 MHz Bruker  
10 Ultrashield spectrometer with  $\text{SiMe}_4$  as the standard. CH-Instruments (model no. CHI6003E)  
11 electrochemical analyser was used to analyse the redox behaviour with Pt as the working and  
12 auxiliary electrodes, saturated calomel electrode (SCE) as the reference electrode and TBAP  
13 (tetrabutylammonium perchlorate) (0.1M) as the supporting electrolyte under a dry nitrogen  
14 atmosphere at 298 K. Calf thymus (CT) DNA (biochemistry grade) was procured from SRL  
15 (India), methyl green, ethidium bromide, Dulbecco's phosphate buffered saline (DPBS),  
16 Dulbecco's modified Eagle medium (DMEM), fetal bovine serum (FBS), trypsin EDTA  
17 solution and antibiotic-antimitotic solution were procured from the Himedia (India). 3-[4,5-  
18 Dimethylthiazol-2-yl]- 2,5-diphenyltetrazolium (MTT) and 4',6-diamidino-2-phenylindole  
19 dihydrochloride (DAPI) were purchased from Sigma-Aldrich (India). For the DNA binding  
20 study, ultrapure water used for the biological assay was obtained through the purification  
21 system Millipore MilliQ Academic.

### 22 **Synthesis of ligands ( $\text{H}_2\text{L}^{1-4}$ )**

23 Substituted aryl hydrazone ligands  $\text{H}_2\text{L}^{1-3}$  were prepared by the condensation of 3-ethoxy-2-  
24 hydroxybenzaldehyde with the corresponding hydrazides [1-naphthoic hydrazide ( $\text{H}_2\text{L}^1$ ), 2-  
25 furoic hydrazide ( $\text{H}_2\text{L}^2$ ) and 2-thiophenecarboxylic acid hydrazide ( $\text{H}_2\text{L}^3$ )], while,  $\text{H}_2\text{L}^4$  was

1 obtained by the condensation of 2-hydroxy-1-naphthaldehyde with isonicotinic hydrazide in  
2 equimolar ratio in EtOH medium by following standard procedures [24,65,74]. The resulting  
3 compounds were then filtered, washed thoroughly with ethanol and dried over fused CaCl<sub>2</sub> in  
4 a desiccator. Elemental analysis results NMR (<sup>1</sup>H and <sup>13</sup>C), UV-Vis and IR data verified their  
5 preparation.

6 **H<sub>2</sub>L<sup>1</sup>**: Yield: 62%. Anal. calcd. for C<sub>14</sub>H<sub>14</sub>N<sub>2</sub>O<sub>4</sub>: C, 61.31; H, 5.14; N, 10.21. Found: C, 61.40;  
7 H, 5.36; N, 10.01. IR (KBr pellet, cm<sup>-1</sup>): 3336 ν(O-H); 2998 ν(N-H); 1657 ν(C=O); 1556  
8 ν(C=N). <sup>1</sup>H NMR (400 MHz, DMSO-*d*<sub>6</sub>): δ 12.13 (s, 1H, -OH), 10.81 (s, 1H, NH), 8.65 (s, 1H,  
9 HC=N-), 7.97–6.72 (m, 6H, aromatic), 4.06 (m, 2H, -OCH<sub>2</sub>), 1.35 (t, 3H, -CH<sub>3</sub>). <sup>13</sup>C NMR  
10 (100 MHz, DMSO-*d*<sub>6</sub>): δ 166.18 (CO-N), 159.18 (N=CH-), 152.36–113.59 (10C, aromatic),  
11 69.33 (-OCH<sub>2</sub>), 19.95 (-CH<sub>3</sub>).

12 **H<sub>2</sub>L<sup>2</sup>**: Yield: 71%. Anal. calcd. for C<sub>20</sub>H<sub>18</sub>N<sub>2</sub>O<sub>3</sub>: C, 71.84; H, 5.43; N, 8.38. Found: C, 71.78;  
13 H, 5.42; N, 8.41. IR (KBr pellet, cm<sup>-1</sup>): 3392 ν(O-H); 3042 ν(N-H); 1657 ν(C=O); 1571  
14 ν(C=N). <sup>1</sup>H NMR (400 MHz, DMSO-*d*<sub>6</sub>): δ 12.02 (s, 1H, -OH), 10.62 (s, 1H, NH), 9.13 (s, 1H,  
15 HC=N-), 8.02–6.97 (m, 10H, aromatic), 4.07 (m, 2H, -OCH<sub>2</sub>), 1.35 (t, 3H, -CH<sub>3</sub>). <sup>13</sup>C NMR  
16 (100 MHz, DMSO-*d*<sub>6</sub>): δ 169.16 (CO-N), 158.67 (N=CH-), 154.16–118.21 (16C, aromatic),  
17 68.31 (-OCH<sub>2</sub>), 14.56 (-CH<sub>3</sub>).

18 **H<sub>2</sub>L<sup>3</sup>**: Yield: 74%. Anal. calcd. for C<sub>14</sub>H<sub>14</sub>N<sub>2</sub>O<sub>3</sub>S: C, 57.92; H, 4.86; N, 9.65; S, 11.04. Found:  
19 C, 57.83; H, 4.91; N, 9.64; S, 10.99. IR (KBr pellet, cm<sup>-1</sup>): 3378 ν(O-H); 2998 ν(N-H); 1663  
20 ν(C=O); 1561 ν(C=N). <sup>1</sup>H NMR (400 MHz, DMSO-*d*<sub>6</sub>): δ 12.11 (s, 1H, -OH), 10.86 (s, 1H,  
21 NH), 8.86 (s, 1H, HC=N-), 7.92–6.98 (m, 6H, aromatic), 4.06 (m, 2H, -OCH<sub>2</sub>), 1.35 (t, 3H, -  
22 CH<sub>3</sub>). <sup>13</sup>C NMR (100 MHz, DMSO-*d*<sub>6</sub>): δ 167.02 (CO-N), 156.23 (N=CH-), 151.52–115.23  
23 (10C, aromatic), 66.34 (-OCH<sub>2</sub>), 16.52 (-CH<sub>3</sub>).

24 **H<sub>2</sub>L<sup>4</sup>**: Yield: 74%. Anal. calcd. for C<sub>17</sub>H<sub>15</sub>N<sub>3</sub>O<sub>2</sub>: C, 69.61; H, 5.15; N, 14.33. Found: C, 69.24;  
25 H, 5.44; N, 14.41. IR (KBr pellet, cm<sup>-1</sup>): 3389 ν(O-H); 2988 ν(N-H); 1653 ν(C=O); 1569

1  $\nu(\text{C}=\text{N})$ .  $^1\text{H}$  NMR (400 MHz,  $\text{DMSO}-d_6$ ):  $\delta$  12.53 (s, 1H,  $-\text{OH}$ ), 12.41 (s, 1H, NH), 9.49 (s, 1H,  
2  $\text{HC}=\text{N}-$ ), 8.85–7.24 (m, 10H, aromatic).  $^{13}\text{C}$  NMR (100 MHz,  $\text{DMSO}-d_6$ ):  $\delta$  166.89 (CO–N),  
3 160.41 (N=CH–), 151.52–114.91(13C, aromatic).

#### 4 **Synthesis of (1)**

5  $[\text{MoO}_2(\text{acac})_2]$  was added to an refluxing solution of  $\text{H}_2\text{L}^1$  (1:1 ratio) taking methanol as the  
6 solvent. The reaction mixture was refluxed for 4 h after which the solution turned dark-orange.  
7 The resultant reaction mixture was filtered and kept for crystallization. After 2-3 days of slow  
8 evaporation, a fine orange crystalline complex,  $[\text{Mo}^{\text{VI}}\text{O}_2\text{L}^1(\text{Q})]$  (where, Q = MeOH) (**1**),  
9 suitable for X-ray crystallographic measurements was obtained.

10  **$[\text{Mo}^{\text{VI}}\text{O}_2\text{L}^1(\text{Q})]$  (**1**):** Yield: 66%. Anal. Calcd for  $\text{C}_{15}\text{H}_{16}\text{MoN}_2\text{O}_7$ : C, 41.68; H, 3.73; N, 6.48;  
11 Found: C, 41.66; H, 3.79; N, 6.51. IR (KBr pellet,  $\text{cm}^{-1}$ ): 1584  $\nu(\text{C}=\text{N})$ , 945, 934  $\nu(\text{Mo}=\text{O})$ .  
12 UV–Vis ( $\text{DMSO}$ ):  $\lambda_{\text{max}}$ , nm ( $\epsilon$ ,  $\text{dm}^3 \text{mol}^{-1} \text{cm}^{-1}$ ): 442 (1011), 310 (9758).  $^1\text{H}$  NMR (400 MHz,  
13  $\text{DMSO}-d_6$ ):  $\delta$  (ppm): 8.89 (s, 1H,  $\text{HC}=\text{N}-$ ), 7.96–6.71 (m, 6H, aromatic), 4.14 (s, 1H,  $-\text{HO}$   
14 (enolic)), 4.096 (m, 2H,  $-\text{OCH}_2$ ), 3.18 (d, 3H,  $-\text{OCH}_3$ ), 1.35 (t, 3H,  $-\text{CH}_3$ ).  $^{13}\text{C}$  NMR (100  
15 MHz,  $\text{DMSO}-d_6$ ):  $\delta$  (ppm): 161.98 (CO=N), 156.32 (N=CH–), 149.78–112.98 (10C, aromatic),  
16 64.82 ( $-\text{OCH}_2$ ), 49.07 ( $-\text{OCH}_3$ ), 15.19 ( $-\text{CH}_3$ ).

#### 17 **Synthesis of mixed-ligand complexes (2–4)**

18 The precursor  $[\text{MoO}_2(\text{acac})_2]$  was added to an refluxing methanolic solution of  $\text{H}_2\text{L}^{2-4}$  in a  
19 equimolar ratio and a dark-orange solution was obtained in each case after 1 h of reflux. Then  
20 a stoichiometric amount of the co-ligand imidazole (Q) was added. Each solution was filtered  
21 after a reflux period of ca 3 h. After slow evaporation of the filtrate over 4 days, orange-red  
22 crystals of  $[\text{Mo}^{\text{VI}}\text{O}_2\text{L}^{2-3}(\text{Q})]$  (**2** and **3**) and  $[\text{Mo}^{\text{VI}}\text{O}_2\text{L}^4(\text{Q})]_2(\text{H}_2\text{O})$  (**4**), were obtained and washed  
23 thoroughly with methanol and dried.

24  **$[\text{Mo}^{\text{VI}}\text{O}_2\text{L}^2(\text{Q})]$  (**2**):** Yield: 68%. Anal. Calcd for  $\text{C}_{23}\text{H}_{22}\text{MoN}_4\text{O}_5$ : C, 52.28; H, 3.82; N, 10.60.  
25 Found: C, 52.17; H, 3.88; N, 10.71. IR (KBr pellet,  $\text{cm}^{-1}$ ): 1567  $\nu(\text{C}=\text{N})$ ; 922, 906  $\nu(\text{Mo}=\text{O})$ .

1 UV-Vis (DMSO):  $\lambda_{\max}$ , nm ( $\epsilon$ ,  $\text{dm}^3 \text{mol}^{-1} \text{cm}^{-1}$ ): 441 (1300), 307 (10124).  $^1\text{H}$  NMR (400  
2 MHz, DMSO- $d_6$ ):  $\delta$  (ppm): 9.06 (s, 1H, HC=N-), 8.83–7.02 (m, 13H, aromatic), 4.12 (m, 2H,  
3 –OCH<sub>2</sub>), 1.38 (t, 3H, –CH<sub>3</sub>).  $^{13}\text{C}$  NMR (100 MHz, DMSO- $d_6$ ):  $\delta$  (ppm): 170.78 (CO=N),  
4 157.32 (N=CH-), 150.10–119.24 (19C, aromatic), 64.83 (–OCH<sub>2</sub>), 15.22 (–CH<sub>3</sub>).

5 **[Mo<sup>VI</sup>O<sub>2</sub>L<sup>3</sup>(Q)] (3)**: Yield: 64%. Anal. Calcd for C<sub>17</sub>H<sub>16</sub>MoN<sub>4</sub>O<sub>5</sub>S: C, 42.16; H, 3.33; N,  
6 11.57; S, 6.62. Found: C, 42.11; H, 3.39; N, 11.58; S, 6.71. IR (KBr pellet,  $\text{cm}^{-1}$ ): 1557  
7  $\nu(\text{C}=\text{N})$ ; 928, 906  $\nu(\text{Mo}=\text{O})$ . UV-Vis (DMSO):  $\lambda_{\max}$ , nm ( $\epsilon$ ,  $\text{dm}^3 \text{mol}^{-1} \text{cm}^{-1}$ ): 442 (1425),  
8 322 (8986).  $^1\text{H}$  NMR (400 MHz, DMSO- $d_6$ ):  $\delta$  (ppm): 8.87 (s, 1H, HC=N-), 7.86–6.99 (m, 6  
9 H, aromatic), 4.07 (m, 2H, –OCH<sub>2</sub>), 1.34 (t, 3H, –CH<sub>3</sub>).  $^{13}\text{C}$  NMR (100 MHz, DMSO- $d_6$ ):  $\delta$   
10 (ppm): 165.90 (CO=N), 155.69 (N=CH-), 150.27–119.71 (10C, aromatic), 65.22 (–OCH<sub>2</sub>),  
11 15.19 (–CH<sub>3</sub>).

12 **[Mo<sup>VI</sup>O<sub>2</sub>L<sup>4</sup>(Q)]<sub>2</sub> (H<sub>2</sub>O) (4)**: Yield: 61%. Anal. Calcd for C<sub>40</sub>H<sub>32</sub>Mo<sub>2</sub>N<sub>10</sub>O<sub>9</sub>: C, 48.60; H, 3.26;  
13 N, 14.17. Found: C, 48.66; H, 3.21; N, 14.18. IR (KBr pellet,  $\text{cm}^{-1}$ ): 1557  $\nu(\text{C}=\text{N})$ ; 928, 906.  
14  $\nu(\text{Mo}=\text{O})$ . UV-Vis (DMSO):  $\lambda_{\max}$ , nm ( $\epsilon$ ,  $\text{dm}^3 \text{mol}^{-1} \text{cm}^{-1}$ ): 453 (2983), 328 (9456), 260  
15 (10531).  $^1\text{H}$  NMR (400 MHz, DMSO- $d_6$ ):  $\delta$  (ppm): 9.82 (s, 1H, HC=N-), 8.79–7.03 (m, 13 H,  
16 aromatic).  $^{13}\text{C}$  NMR (100 MHz, DMSO- $d_6$ ):  $\delta$  (ppm): 166.87 (CO=N), 161.33 (N=CH-),  
17 154.31–112.00 (16C, aromatic).

## 18 **Single crystal X-ray structure determination**

19 Crystal data and refinement details for **1-4** are collated in Table 1. Intensity data (100 K) for  
20 **1-3** were measured on a Rigaku/Oxford Diffraction XtaLAB Synergy diffractometer (Dualflex,  
21 AtlasS2) fitted with CuK $\alpha$  radiation ( $\lambda = 1.54178 \text{ \AA}$ ) while those for **4** were measured on an  
22 Agilent Technologies SuperNova Dual CCD with an Atlas detector fitted with Mo K $\alpha$  radiation  
23 ( $\lambda = 0.71073 \text{ \AA}$ ). Data reduction and empirical absorption corrections, based on a gaussian (**1-**  
24 **3** [80]) or multi-scan (**4** [81]) techniques, were applied. The structures were solved by direct  
25 methods [82] and refined on  $F^2$  with anisotropic displacement parameters and C-bound H



1 atoms in the riding model approximation [83]. For **1**, the oxygen-bound H atoms were refined  
2 with a distance restraint O–H = 0.84±0.01 Å while for **2-4**, the nitrogen-bound H atoms were  
3 refined with a distance restraint N–H = 0.88±0.01 Å. A weighting scheme of the form  $w =$   
4  $1/[\sigma^2(F_o^2) + (aP)^2 + bP]$  where  $P = (F_o^2 + 2F_c^2)/3$  was introduced in each refinement. For **2**,  
5 the maximum and minimum residual electron density peaks of 2.69 and 1.03 eÅ<sup>-3</sup>, respectively,  
6 were located 0.84 and 0.72 Å from the Mo atom, respectively. This is an artefact of the data  
7 and not indicative of unresolved chemistry. For **3**, owing to poor agreement, the (1 1 3)  
8 reflection was omitted from the last cycles of refinement. The thienyl ring was disordered over  
9 two co-planar, anti-parallel orientations with the site occupancy factor of the major component  
10 refining to 0.875(4). The C9, C11 and C12 positions were common to both components and  
11 were refined anisotropically. The S1 and C10 atoms of the major component were refined  
12 anisotropically but those for the minor component were refined isotropically. The C9–C10 and  
13 C10–C11 bond lengths of the minor component were constrained to be equivalent to those for  
14 the major component. Finally, the absolute structure was determined based on differences in  
15 Friedel pairs included in the data set. In **4**, there is half a water molecule disordered over two  
16 positions about a centre of inversion; the O–H distances were fixed at 0.84 Å. There is some  
17 evidence for disorder in the imidazole ring as seen in the shapes of the displacement ellipsoids.  
18 However, an alternate position was not discerned for this molecule. The molecular structure  
19 diagrams were generated by ORTEP for Windows [84] and the packing diagrams with  
20 DIAMOND [85]. Additional data analysis was made with PLATON [86].

1 Table 1. Crystal data and refinement details for complexes **1-4**.

2	Complex	<b>1</b>	<b>2</b>	<b>3</b>	<b>4</b>
3	Formula	C <sub>15</sub> H <sub>16</sub> MoN <sub>2</sub> O <sub>7</sub>	C <sub>23</sub> H <sub>20</sub> MoN <sub>4</sub> O <sub>5</sub>	C <sub>17</sub> H <sub>16</sub> MoN <sub>4</sub> O <sub>5</sub> S	C <sub>40</sub> H <sub>32</sub> Mo <sub>2</sub> N <sub>10</sub> O <sub>9</sub>
4	Formula weight	432.24	528.37	484.34	988.64
5	Crystal colour	light-brown	light-brown	light-brown	red-brown
6	Crystal size/mm <sup>3</sup>	0.08 × 0.10 × 0.11	0.03 × 0.04 × 0.08	0.13 × 0.16 × 0.17	0.10 × 0.25 × 0.30
7	Crystal system	Triclinic	Triclinic	Orthorhombic	Monoclinic
8	Space group	<i>P</i> $\bar{1}$	<i>P</i> $\bar{1}$	<i>P</i> 2 <sub>1</sub> 2 <sub>1</sub>	<i>P</i> 2 <sub>1</sub> / <i>n</i>
9	<i>a</i> /Å	10.2487(2)	7.98370(10)	8.09320(10)	9.4568(2)
10	<i>b</i> /Å	12.2450(2)	9.8896(2)	12.0195(2)	13.0259(2)
11	<i>c</i> /Å	13.2350(4)	13.9897(2)	19.6535(2)	15.9707(3)
12	$\alpha$ /°	90.236(2)	91.2290(10)	90	90
13	$\beta$ /°	97.070(2)	90.0870(10)	90	106.320(2)
14	$\gamma$ /°	90.6870(10)	104.721(2)	90	90
15	<i>V</i> /Å <sup>3</sup>	1648.16(7)	1068.03(3)	1911.82(4)	1888.05(6)
16	<i>Z</i>	4	2	4	2

1	$D_c/g\text{ cm}^{-3}$	1.742	1.643	1.683	1.739
2	$F(000)$	872	536	976	996
3	$\mu(\text{MoK}\alpha)/\text{mm}^{-1}$	6.901	5.410	6.972	0.738
4	Measured data	39123	25342	13028	9628
5	$\theta$ range/ $^\circ$	3.4 – 67.1	3.2 – 67.1	4.3 – 67.1	2.3 – 29.3
6	Unique data	5893	3817	3399	4403
7	Observed data ( $I \geq 2.0\sigma(I)$ )	5652	3707	3386	3665
8	No. parameters	461	302	266	283
9	$R$ , obs. data; all data	0.022; 0.059	0.037; 0.096	0.019; 0.047	0.031; 0.074
10	$a$ ; $b$ in weighting scheme	0.039; 1.022	0.052; 2.843	0.030; 0.698	0.037; 2.383
11	$R_w$ , obs. data; all data	0.023; 0.600	0.038; 0.097	0.019; 0.047	0.043; 0.083
12	Range of residual electron				
13	density peaks/ $\text{e}\text{\AA}^{-3}$	-0.74 – 0.42	-1.03 – 2.69	-0.65 – 0.26	-0.57–0.63

---

## 1 DNA binding experiments

### 2 Absorption spectral studies

3 Interaction of the dioxidomolybdenum(VI) complexes with CT-DNA was studied through UV-  
4 Vis absorption titration experiments. A fixed concentration of the metal complex (25  $\mu\text{M}$ ) was  
5 titrated against a variable concentration of CT-DNA (0 to 110  $\mu\text{M}$ ) in 50 mM Tris-HCl buffer  
6 (pH 8.0). Readings were recorded after each addition of CT-DNA (10  $\mu\text{M}$ ) to the metal. Data  
7 were then calculated using the following equation (Eqn 1) to obtain the binding constant  $K_b$   
8 [37,66,73]

$$9 \quad \frac{[DNA]}{\epsilon_a - \epsilon_f} = \frac{[DNA]}{\epsilon_b - \epsilon_f} + \frac{1}{K_b(\epsilon_b - \epsilon_f)} \quad (\text{Eqn 1})$$

10 where [DNA] is represents the concentration of CT–DNA base pairs whereas the parameters  
11  $\epsilon_a$ ,  $\epsilon_f$  and  $\epsilon_b$  correspond to the apparent extinction co-efficient for the complexes, i.e.  
12 Abs/[complex] in the presence and absence of CT–DNA and to fully bound DNA, respectively.  
13 A plot of  $[DNA]/(\epsilon_a - \epsilon_f)$  vs [DNA] gave a slope of  $1/(\epsilon_a - \epsilon_f)$  and the intercept equal to  
14  $(1/K_b)(\epsilon_b - \epsilon_f)$ . Thus, the ratio of the slope to the intercept gives the value of binding constant  
15  $K_b$ . Binding affinity of the ligands towards CT-DNA was studied in a similar fashion by taking  
16 a fixed concentration of ligand [25  $\mu\text{M}$  in 50 mM Tris-HCl buffer (pH 8.0)] against variable  
17 CT-DNA concentrations ranging from 0 to 100  $\mu\text{M}$ .

### 18 Competitive DNA binding by Fluorescence measurements

19 To understand the exact mode of binding of the complexes with CT-DNA, competitive DNA  
20 binding experiments with three fluorescent dyes namely 4',6-diamidino-2-phenylindole  
21 (DAPI), methyl green (MG) and ethidium bromide (EB) was carried out. Among these  
22 fluorescent dyes EB tends to bind DNA through intercalation whereas DAPI and MG bind to  
23 the minor and major grooves, respectively [66,87,88]. This was studied by measuring the  
24 fluorescence emission intensities of DAPI, MG and EB bound CT-DNA at 455 nm (excitation  
25 358 nm), 663 nm (excitation 600 nm) and 597 nm (excitation 520 nm) with an increasing

1 amount of the complex concentration (0–100  $\mu$ M) in a Fluoromax 4P spectrofluorimeter  
2 (Horiba Jobin Mayer, USA).

### 3 ***In vitro* cytotoxic activity**

#### 4 **Cell cultures**

5 HT-29 (colon cancer) and HeLa (cervical cancer) cells were obtained from National Centre of  
6 Cell Science (NCCS), Pune, India. The cells were maintained in DMEM supplemented with  
7 10% FBS and penicillin–streptomycin solution at 37 °C in a 95% humidified and 5% CO<sub>2</sub>  
8 incubator. Working concentrations of 5, 10, 50 and 100  $\mu$ g/ml were prepared in culture medium  
9 from a stock concentration of 3 mg/ml of each complex. Also, the concentration of DMSO was  
10 maintained at less than 0.1% (v/v) in all experiments to avoid any toxicity due to DMSO.

#### 11 **MTT assay**

12 For the MTT assay, both HT-29 and HeLa cells were harvested from their maintenance cultures  
13 in logarithmic phase. Following cell counting in a hemocytometer, cells were seeded into a 96  
14 well plate, at a concentration of  $1 \times 10^4$  cells per well. These cells were then incubated with  
15 various concentrations of the test compounds for 48 h. The result of the treatment of the  
16 complexes on viability of the cancer cells was studied using MTT dye reduction assay by  
17 measuring the optical density at 595 nm using micro-plate reader spectrophotometer (Perkin-  
18 Elmer 2030) [78].

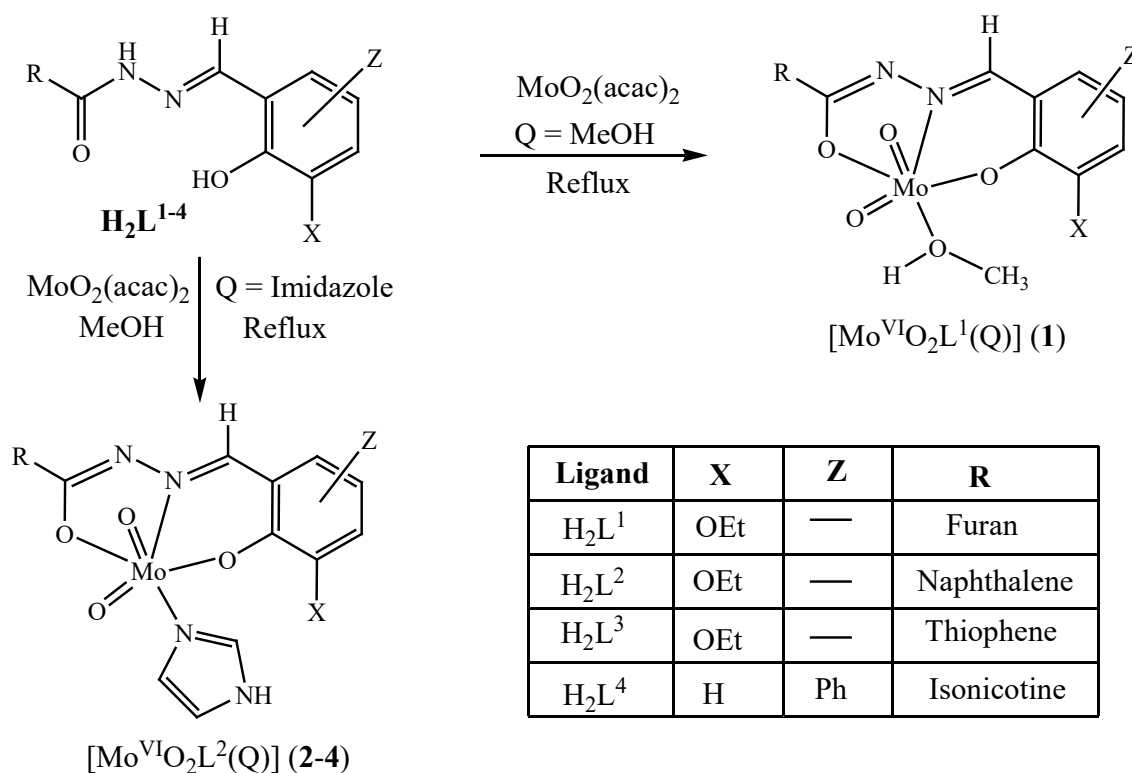
#### 19 **DAPI staining**

20 Nuclear morphology of the cancer cells in response to treatment with the complexes was  
21 studied through DAPI staining by following a reported procedure [68]. Treated and untreated  
22 cells were fixed with 4 % formaldehyde for 15 min followed by staining with 1  $\mu$ g/ml DAPI  
23 for 5 min at 37 °C. The cells were then washed with PBS and finally examined by fluorescence  
24 microscopy (Olympus IX 71) to determine if any nuclear condensation or fragmentation had  
25 occurred, indicating the cells underwent apoptosis.

## 1 Results and discussion

### 2 Synthesis

3 In the present study, four new mixed ligand dioxidomolybdenum(VI)  $[\text{Mo}^{\text{VI}}\text{O}_2\text{L}^{1-3}(\text{Q})]$  (**1–3**),  
4  $[\text{Mo}^{\text{VI}}\text{O}_2\text{L}^4(\text{Q})]_2 (\text{H}_2\text{O})$  (**4**) [where Q = MeOH for **1** and imidazole for **2–4**] complexes were  
5 synthesized from four differently substituted ONO donor aroylhydrazone ligands,  $\text{H}_2\text{L}^{1-4}$ , as  
6 indicated in Scheme 1. The complexes were successfully characterized by UV–vis, IR, NMR,  
7 cyclic voltammetry and the molecular and crystal structures were determined by X-ray  
8 crystallography. The aqueous phase stability of the complexes has been investigated by time-  
9 dependent UV-vis spectroscopy for 72h and a representative spectrum, for **1**, is depicted in Fig.  
10 SI 1.



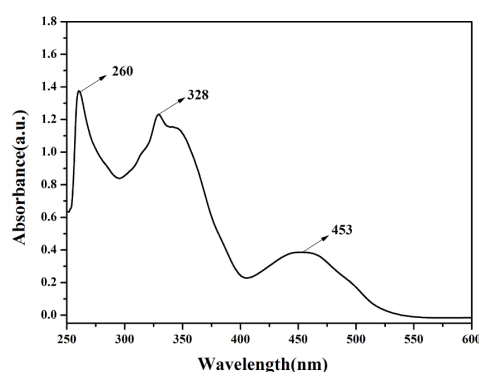
11

12 **Scheme 1.** Schematic pathway for the formation of  $[\text{Mo}^{\text{VI}}\text{O}_2\text{L}^{1-3}(\text{Q})]$  (**1–3**),  
13  $[\text{Mo}^{\text{VI}}\text{O}_2\text{L}^4(\text{Q})]_2 (\text{H}_2\text{O})$  (**4**).

### 14 Spectral characteristics

1 Detailed spectral (IR, UV-Vis and NMR) data of  $H_2L^{1-4}$  and their respective corresponding  
2 complexes (**1–4**) are given in the *Experimental section*. Infrared spectra of the ligands display  
3 three broad band in the ranges 3392–3336, 3042–2988 and 1663–1653  $cm^{-1}$  which are  
4 attributed to  $\nu(O-H)$  stretching of hydroxy group of 2-hydroxy aldehyde,  $\nu(N-H)$  stretching  
5 and  $\nu(C=O)$  stretching, respectively. Disappearance of characteristic bands of O–H, N–H and  
6 C=O in the complex spectra indicates the coordination of the ligands to the metal centre in their  
7 phenolate form after enolization [77,89]. Also, the presence of two new stretching bands in the  
8 range 928–906  $cm^{-1}$  in the complex spectra indicate the dioxido nature (Mo=O) of the  
9 complexes.

10 Electronic spectra of **1–4** were recorded in DMSO. The spectra of all the complexes were  
11 similar in nature and as a representative UV-Vis spectrum of **4** is depicted in Fig. 1. Strong  
12 absorptions observed in the range 453–442 nm are assignable to ligand-to-metal charge transfer  
13 (LMCT) transitions whereas bands in the higher energy region 328–260 nm are likely to be  
14 due to ligand centred transitions [75,77]. Moreover, the presence an extra peak in the complex  
15 spectra at 453–442 nm region, as compared to that of the ligand suggests coordination of the  
16 ligand upon complexation.



17  
18 **Fig. 1.** UV-vis spectra of  $[Mo^{VI}O_2L^4(Q)]_2.H_2O$  (**4**) in DMSO employing the complex  
19 concentration  $1.3 \times 10^{-4}$  M.

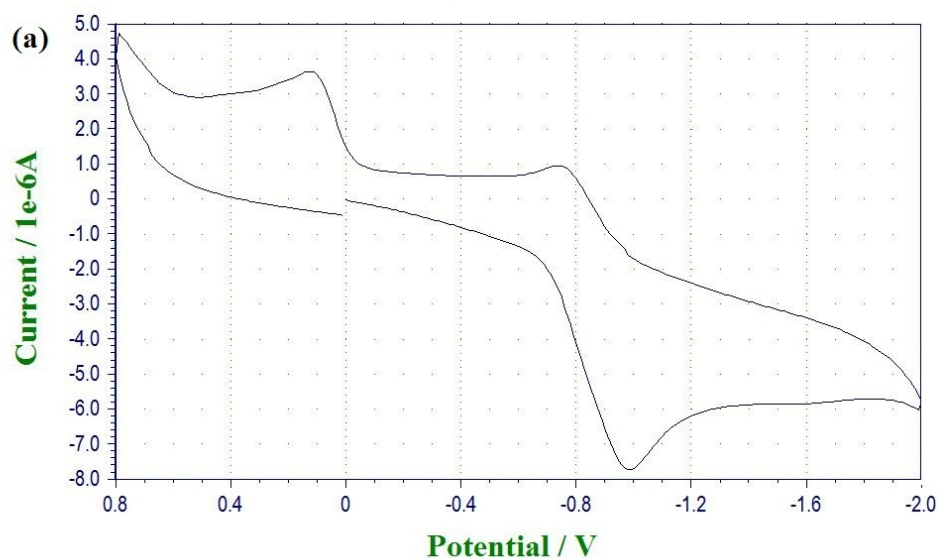
1 The  $^1\text{H}$  and  $^{13}\text{C}$  NMR data of  $\text{H}_2\text{L}^{1-4}$  and their corresponding complexes (**1–4**) were recorded  
2 in  $\text{DMSO}-d_6$ . The ligand spectra exhibit two singlets in the ranges  $\delta = 12.53\text{--}12.02$  and  $12.41\text{--}$   
3  $10.62$  ppm due to the presence of phenolic  $\text{--OH}$  and  $\text{NH}$  protons, respectively. The  
4 disappearance of these two resonances in the spectra of the complexes confirms their  
5 deprotonation and coordination to the central metal atom. The presence of a singlet resonance  
6 for the ligands and complexes in the region  $\delta = 9.82\text{--}8.65$  ppm is attributed to the azomethine  
7  $\text{--CH}$  proton. One quartet in the range  $\delta = 4.12\text{--}4.06$  ppm and a triplet in the range  $\delta = 1.38\text{--}$   
8  $1.34$  ppm is observed for  $\text{H}_2\text{L}^{1-3}$  and their complexes **1–3** due to the presence of the ethoxy  
9 group in the ligand moiety. On the other hand, due to presence of a coordinated  $\text{MeOH}$   
10 molecule, complex **1** exhibits an  $\text{OH}$  (enolic) resonance at  $\delta = 4.14$  ppm and a  $\text{--OCH}_3$   
11 resonance at  $\delta = 4.09$  ppm. Moreover, the increased number of resonances in the aromatic  
12 region for complexes **2–4** as compared to  $\text{H}_2\text{L}^{2-4}$  indicates the binding of co-ligand imidazole  
13 to the metal atom.  $^1\text{H}$  NMR spectra of all the complexes (**1–4**) are given in Figs SI 2–5.  
14 In the  $^{13}\text{C}$  NMR spectra of **1–4**, signals for the aromatic carbons are found in the downfield  
15 region in the range  $\delta = 170.78\text{--}112.98$  ppm. Signals for the aliphatic carbons of  $\text{--OCH}_2$  and  $\text{--}$   
16  $\text{CH}_3$  of **1–3** appear in the range  $\delta = 65.22\text{--}15.19$  ppm. Whereas complex **1** exhibits an additional  
17 aliphatic carbon signal at  $\delta = 49.07$  due to the presence of methanolic  $\text{--OCH}_3$  carbon.

## 18 **Electrochemical Properties**

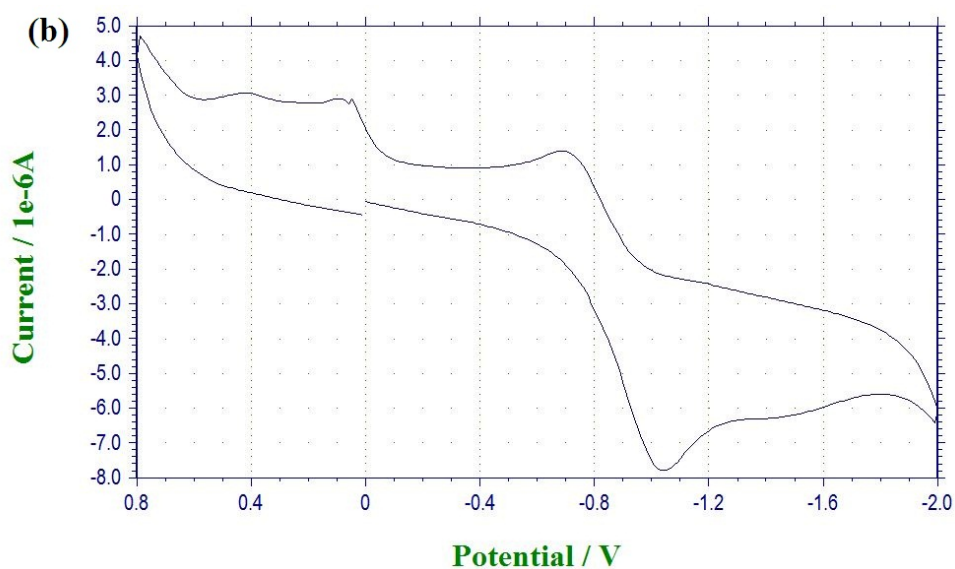
19 Electrochemical properties of the complexes have been studied by cyclic voltammetry in  
20  $\text{DMSO}$  solution. Voltammograms of all the complexes show a similar type of redox property  
21 and representative voltammograms for **1** and **2** are depicted in Fig. 2. An irreversible single  
22 electron reductive response is observed in the cathodic region at a potential window  $\text{--}0.74$  to  
23  $\text{--}0.69$  V that can be attributed to the  $\text{Mo(VI)} \rightarrow \text{Mo(V)}$  reduction [68,74,76,90]. Also, a single  
24 electron irreversible cathodic response in the region  $\text{--}1.04$  to  $\text{--}0.95$  V and anodic response at a  
25 potential window  $0.44$  to  $0.12$  V are observed that may be attributed to the ligand centered



1 reduction and oxidation, respectively. The cyclic voltammetry experiments of the ligands have  
2 also been performed and a representative voltammogram of H<sub>2</sub>L<sup>1</sup> is shown in Fig. SI 6. The  
3 redox potential data of all the complexes are listed in Table 2 and the single electron processes  
4 were also confirmed by comparing the current height to the standard ferrocene–ferrocenium  
5 couple under identical experimental conditions.



6



7

8 **Fig. 2.** Cyclic voltammogram of [Mo<sup>VI</sup>O<sub>2</sub>L<sup>1</sup>(Q)] (**1**) (a) and [Mo<sup>VI</sup>O<sub>2</sub>L<sup>2</sup>(Q)] (**2**) (b) in  
9 DMSO.

10 **Table 2.** Cyclic voltammetric results<sup>a</sup> for **1–4** at 298 K in DMSO.

Complex	E <sup>c</sup> <sub>P</sub> (V)	E <sup>a</sup> <sub>P</sub> (V)
1	-0.74, -0.99	0.12
2	-0.69, -1.04	0.39
3	-0.71, -1.04	0.21
4	-0.70, -0.95	0.44

1     <sup>a</sup> In DMSO at a scan rate 100 mV s<sup>-1</sup>. Where E<sup>c</sup><sub>P</sub> and E<sup>a</sup><sub>P</sub> are cathodic and anodic peak  
2     potentials vs. SCE, respectively.

### 3     **Molecular structures**

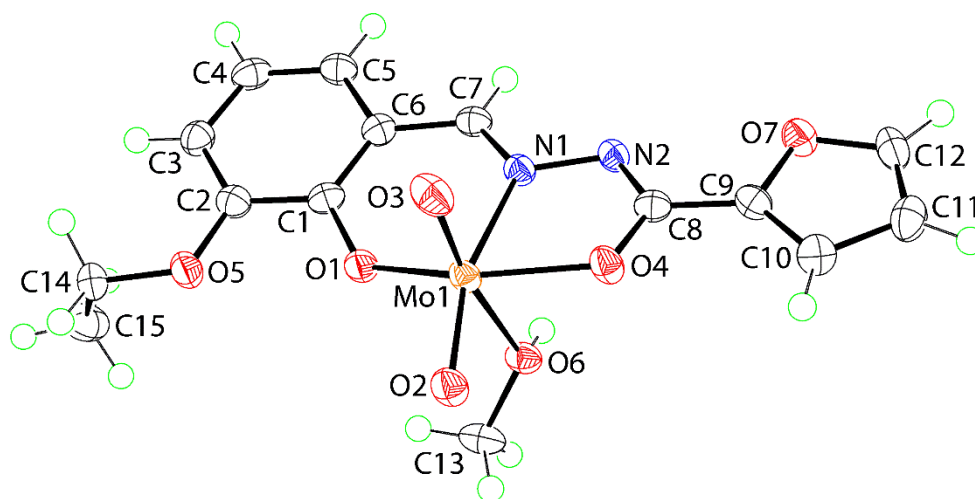
4     The molecular structures of **1-4** have been established by X-crystallography and selected  
5     geometric parameters are collated in Table 3. The crystallographic asymmetric unit of **1**  
6     comprises two independent molecules, the first of which is shown in Fig. 3(a) and the second  
7     in Fig. SI 7(a); the molecules have very similar conformations as seen in the overlay diagram  
8     of Fig. SI 7(b). The **molecules of 1 comprise** a Mo(=O)<sub>2</sub> core complexed by a di-negative,  
9     tridentate Schiff base ligand, via the phenoxide-O1, amide-O4 and imine-N1 atoms, with the  
10    sixth site occupied by an O-bound methanol molecule. The oxo groups **are cis**, the phenoxide-  
11    O1 and amide-O4 atoms trans, the oxido-O2 atom, occupying a position in the approximate  
12    plane of the tridentate ligand, is trans to the imine-N1 atom, and the oxido-O3 atom is trans to  
13    the methanol-O6 atom. The resulting NO<sub>5</sub> donor set is based on an octahedron. The mode of  
14    coordination of the tridentate ligand gives rise to five- and six-membered chelate rings and it  
15    is the acute bite angles subtended by these (Table 3) that are responsible for the major  
16    distortions from the ideal octahedral geometry.

17    The Mo-O1(phenoxide) bond length of 1.9170(14) Å is considerably shorter than the Mo-  
18    O4(amide) bond length of 2.0299(14) Å, an observation correlated with delocalisation of π-  
19    electron density over the amide chromophore. ~~While the differences in the geometric~~

1 parameters involving the lighter atoms are small, there are discernible and consistent trends to  
2 substantiate this observation. Thus, the C8–O4 bond length is significantly shorter than the  
3 C1–O1 bond, i.e. 1.312(2) Å cf. 1.351(2) Å, and conversely, there is an indication the formally  
4 double C8–N2 bond is longer, at 1.309(3) Å, than the C7–N1 imine bond, at 1.295(3) Å, the  
5 experimental errors notwithstanding. In the same way, there is an indication that the Mo–  
6 O2(oxido) bond length is longer than the Mo–O3(oxido) bond, i.e. 1.7083(13) Å cf. 1.6956(15)  
7 Å, with the former being trans to the imine-N1 atom, and the latter trans to the methanol-O6  
8 atom. Delete to make the text shorter? I obviously think this is important but, perhaps it is too  
9 detailed for the Journal's liking

10 As mentioned above, the five-membered, i.e. Mo,O4,N1,N2,C8, and six-membered, i.e.  
11 Mo,O1,C1,C6,C7,N1, chelate rings are formed upon complexation of the di-anion. The five-  
12 membered ring is practically planar, exhibiting a r.m.s. deviation for the five atoms of 0.0087  
13 Å. By contrast, the best description for the six-membered ring is that of an envelope whereupon  
14 the Mo1 atom lies 0.504(2) Å out of the plane of the five remaining atoms, which exhibit a  
15 r.m.s. deviation of 0.0435 Å. The dihedral angle between the least-squares planes through the  
16 chelate rings is 7.82(9)°, indicating the backbone of the tridentate ligand is approximately  
17 planar. The appended furanyl ring makes a dihedral angle of 6.11(13)° with the five-membered  
18 chelate ring, again indicating a co-planar arrangement; the dihedral angle between the outer  
19 rings is 5.26(14)°.

20



1

2 **Fig. 3.** Molecular structure of the first independent molecule comprising the asymmetric unit  
 3 of **1**, showing **the atom** labelling scheme and anisotropic displacement parameters at the 70%  
 4 probability **level.**

5

6

7

8

9

10

11

12

13

14

15 **Table 3.** Selected geometric parameters (Å, °) for complexes **1-4**.

16 Complex	<b>1</b>	<b>1<sup>a</sup></b>	<b>2</b>	<b>3</b>	<b>4</b>
17	(Y = O6)	(Y = O6)	(Y = N3)	(Y = N3)	(Y = N3)
18 Parameter					
19 Mo–O1	1.9170(14)	1.9242(14)	1.947(2)	1.947(2)	1.9367(17)
20 Mo–O2	1.7083(13)	1.7068(13)	1.714(3)	1.709(2)	1.7064(18)

1	Mo–O3	1.6956(15)	1.6966(15)	1.701(3)	1.698(2)	1.7040(19)
2	Mo–O4	2.0299(14)	2.0351(14)	2.010(2)	2.016(2)	2.0169(19)
3	Mo–N1	2.2457(16)	2.2423(16)	2.231(3)	2.248(2)	2.228(2)
4	Mo–Y	2.3207(14)	2.3221(14)	2.347(3)	2.330(2)	2.336(2)
5	O1–C1	1.351(2)	1.347(2)	1.357(4)	1.353(4)	1.343(3)
6	O4–C	1.312(2)	1.314(2)	1.327(4)	1.322(4)	1.320(3)
7	N1–N2	1.395(2)	1.391(2)	1.403(4)	1.393(3)	1.403(3)
8	N1–C	1.295(3)	1.296(3)	1.275(5)	1.296(4)	1.291(3)
9	N2–C	1.309(3)	1.308(3)	1.293(5)	1.307(4)	1.297(3)
10	O1–Mo–O4	150.17(6)	149.39(6)	149.59(10)	149.33(8)	148.77(8)
11	O1–Mo–N1	81.27(6)	80.85(6)	81.66(10)	81.61(9)	80.41(7)
12	O2–Mo–O3	106.63(7)	105.78(7)	105.94(13)	104.69(10)	106.42(10)
13	O2–Mo–N1	157.75(6)	157.86(6)	161.21(12)	163.61(9)	161.96(9)
14	O3–Mo–Y	169.24(6)	171.72(6)	169.43(12)	170.54(10)	168.97(9)
15	O4–Mo–N1	72.09(6)	71.49(5)	71.77(10)	71.93(9)	72.25(7)

16 <sup>a</sup> The parameters for the second independent molecule in **1** follow the numbering scheme  
 17 shown in Fig. 3(a).

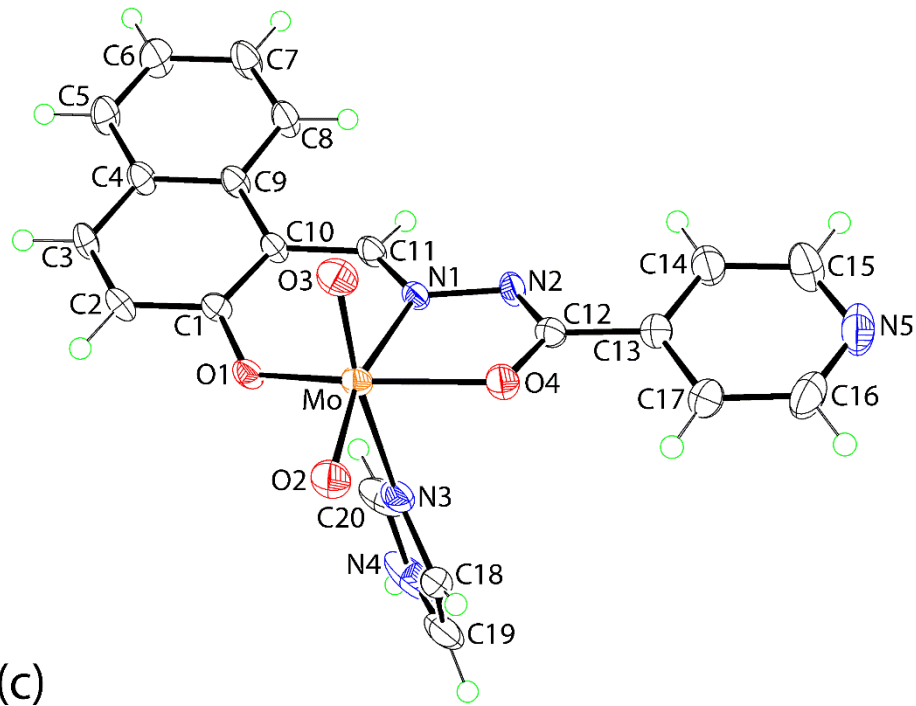
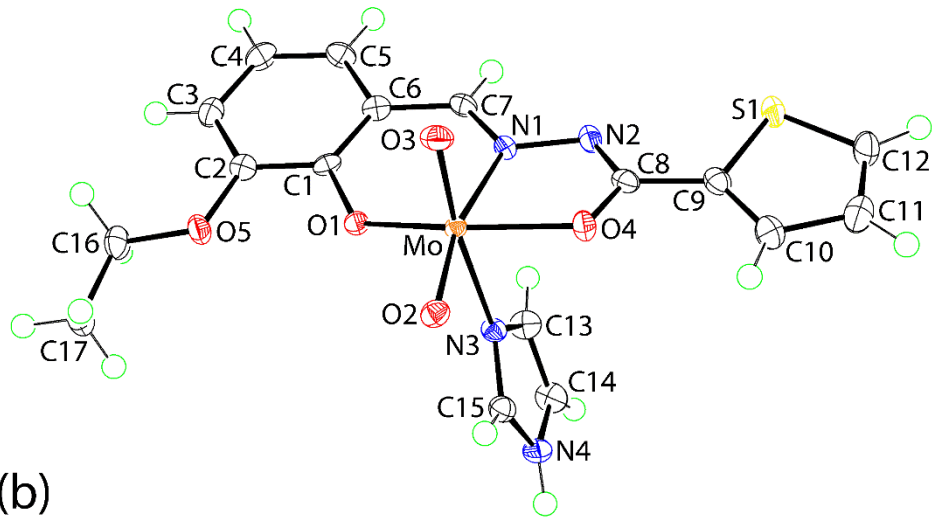
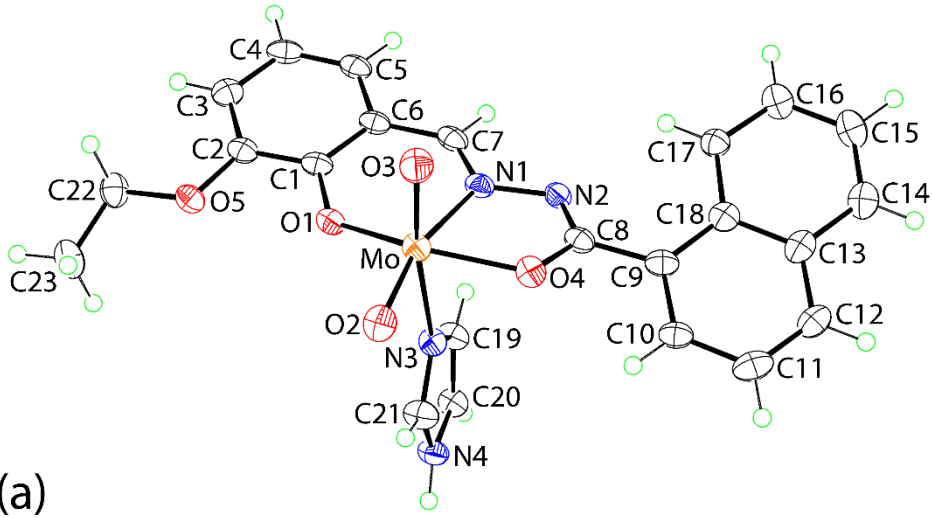
18

19 ~~The second molecule comprising the asymmetric of **1** adopts essentially the same molecular~~  
 20 ~~structure and trends as for the first. The envelope conformation for the six-membered ring is~~  
 21 ~~more pronounced with the Mo2 atom lying 0.603(2) Å out of the plane of the five remaining~~  
 22 ~~atoms (r.m.s. deviation = 0.0367 Å). The dihedral angle between the chelate rings is 9.45(9)°;~~  
 23 ~~between the five-membered and furanyl rings 3.02(12)° and between the outer rings~~  
 24 ~~13.67(12)°, mirroring the first independent molecule. and/or delete this?~~

25 The molecular structures of **2** and **3** are closely related to that of **1** in that the methanol molecule  
 26 has been replaced by an imidazole in each case, and with the furanyl substituent in **1** replaced  
 27 by naphthyl (**2**) and thienyl (**3**), leading to cis-N<sub>2</sub>O<sub>4</sub> distorted octahedral geometries. In **4**,  
 28 imidazole is still present but both peripheral aromatic systems differ, being based on naphthyl  
 29 and 4-pyridyl; **4** was isolated as a mono-hydrate. The molecular structures of **2-4** are shown in

1 Figs 4(a)-(c) and selected geometric parameters are given in Table 3. The molecular geometry  
2 and trends in geometric parameters for **2-4** match closely those established for **1**. The notable  
3 exception is the equivalence of the Mo-O(oxido) bond lengths in **4**. The conformations of the  
4 chelate rings also match those seen in **1**; geometric data are given in Table SI 1. Across the  
5 series, the five-membered rings are most planar in the structures of **2** and **3**, and in terms of the  
6 deviations of the Mo atoms in the envelope conformations for the six-membered rings, these  
7 are intermediate to those seen in the independent molecules of **1**. In the same way, the dihedral  
8 angles between the chelate rings in each of **2-4** are intermediate to those seen in **1**. The dihedral  
9 angles between the outer aromatic rings is greater than those in **1** in the case of **2**, i.e.  
10  $14.77(11)^\circ$ , or smaller, in **3** ( $2.13(17)^\circ$ ) and **4** ( $4.77(19)^\circ$ ).

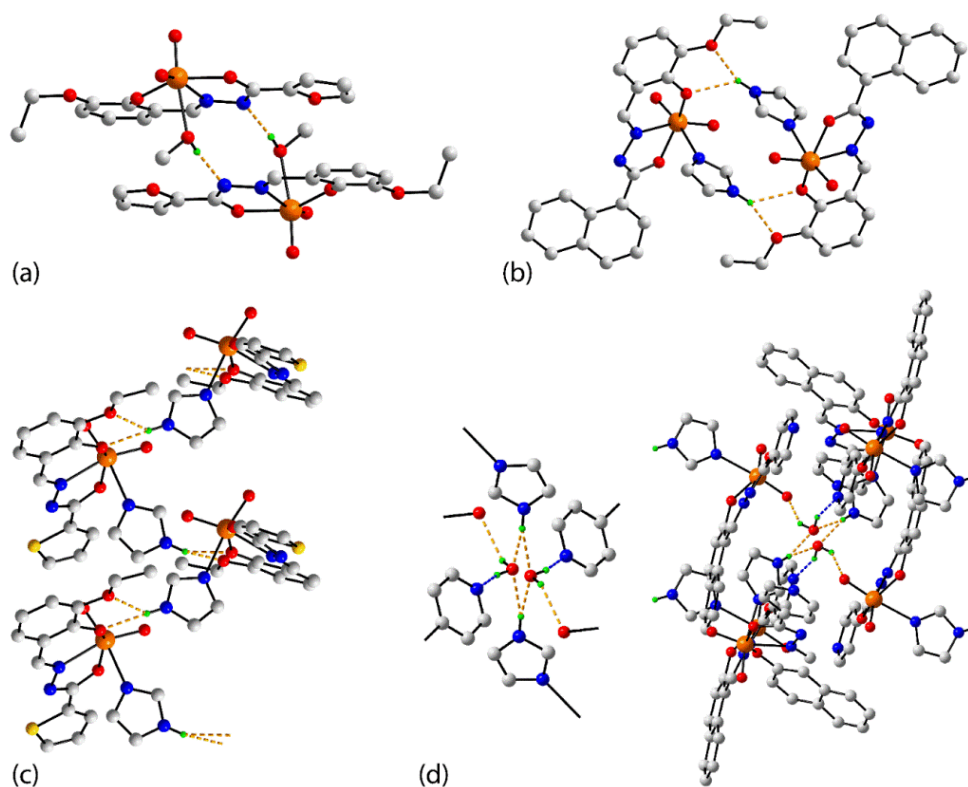
11



1 **Fig. 4.** Molecular structures of (a) **2**, (b) **3** (minor component of the disordered thienyl ring is  
2 omitted) and (c) **4** (water molecule omitted) showing atom labelling schemes and displacement  
3 parameters at the 50, 70 and 50% probability levels, respectively.

#### 4 **Molecular packing**

5 The geometric parameters associated with the specified intermolecular interactions discussed  
6 in the following are collated in the respective captions of **Figs 5 and SI 8-11**. In the molecular  
7 packing of **1**, each independent molecule self-associates into a dimeric aggregate via hydroxy-  
8 O–H···N(imine) hydrogen bonds as shown in Fig. 5(a) and Fig. SI 8(a) for the first and second  
9 independent molecules, respectively. The supramolecular dimers are assembled into a layer in  
10 the ab-plane via furanyl- and imine-C–H···O(oxido) interactions occurring between Mo1- and  
11 Mo2-containing molecules, Fig. SI 8(b). The layers inter-digitate along the c-axis with the  
12 closest atom-to-atom contact being a weak methyl-C–H···O(oxido) contact, Fig. SI 8(c).



13  
14 **Fig. 5.** Supramolecular aggregates in the crystals of **1-4** sustained by hydrogen bonding (shown  
15 as orange dashed lines): (a) dimer in **1** stabilised by hydroxy-O–H···N(imine) hydrogen bonds  
16 [O6–H6o···N2<sup>i</sup>: H6o···N2<sup>i</sup> = 1.907(19) Å, O6···N2<sup>i</sup> = 2.732(2) Å with angle at H6o = 168(2)° for



1 symmetry operation (i) 2-x, 2-y, 1-z], (b) dimer in **2** mediated by imidazole-N-H $\cdots$ O(phenoxide,  
2 ethoxy) hydrogen bonds [N4-H4n $\cdots$ O1<sup>ii</sup>: H4n $\cdots$ O1<sup>ii</sup> = 2.28(3) Å, N4 $\cdots$ O1<sup>ii</sup> = 2.953(4) Å with  
3 angle at H4n = 133(4)°; N4-H4n $\cdots$ O5<sup>ii</sup>: H4n $\cdots$ O5<sup>ii</sup> = 2.26(3) Å, N4 $\cdots$ O5<sup>ii</sup> = 2.983(4) Å with angle  
4 at H4n = 139(4)° for (ii) 1-x, 1-y, 1-z], (c) helical chain in **3** sustained by imidazole-N-  
5 H $\cdots$ O(phenoxide, ethoxy) hydrogen bonds [N4-H4n $\cdots$ O1<sup>iii</sup>: H4n $\cdots$ O1<sup>iii</sup> = 2.19(3) Å, N4 $\cdots$ O1<sup>iii</sup> =  
6 2.947(3) Å with angle at H4n = 144(3)°; N4-H4n $\cdots$ O5<sup>iii</sup>: H4n $\cdots$ O5<sup>iii</sup> = 2.23(3) Å, N4 $\cdots$ O5<sup>iii</sup> =  
7 2.927(3) Å with angle at H4n = 136(3)° for (iii) -1/2+x, 1/2-y, 1-z] and (d) detailed view and seven-  
8 molecule aggregate in **4** sustained by imidazole-N-H $\cdots$ O(water), water-O-H $\cdots$ O(oxido) and  
9 water-O-H $\cdots$ N(pyridyl) hydrogen bonds [O1w-H1w $\cdots$ O3<sup>iv</sup>: H1w $\cdots$ O3<sup>iv</sup> = 2.30 Å, O1w $\cdots$ O3<sup>iv</sup> =  
10 3.028(5) Å with angle at H1w = 145°; O1w-H2w $\cdots$ N5<sup>v</sup>: H2w $\cdots$ N5<sup>v</sup> = 1.91 Å, O1w $\cdots$ N5<sup>v</sup> =  
11 2.708(5) Å with angle at H2w = 158°; N4-H4n $\cdots$ O1w: H4n $\cdots$ O1w = 1.93(2) Å, N4 $\cdots$ O1w =  
12 2.795(7) Å with angle at H2w = 170(4)°; N4-H4n $\cdots$ O1w<sup>vi</sup>: H4n $\cdots$ O1w<sup>vi</sup> = 2.16(3) Å, N4 $\cdots$ O1w<sup>vi</sup>  
13 = 3.016(7) Å with angle at H4n = 166(5)° for (iv) 1/2-x, -1/2+y, 1/2-z, (v) 1/2+x, 1/2-y, -1/2+z and (vi)  
14 -x, -y, -z]; the latter are shown as blue dashed lines. For reasons of clarity, non-participating  
15 hydrogen atoms are removed. {full page image}

16 Centrosymmetric supramolecular dimers are also found in the crystal of **2**. Here, the imidazole-  
17 N-H atom is bifurcated forming hydrogen bonds with the phenoxide-O1 and ethoxy-O5 atoms  
18 to form a five-membered { $\cdots$ H $\cdots$ OC<sub>2</sub>O} synthon, Fig. 5(b). Each component of the dimer is  
19 connected into a layer in the ab-plane by naphthyl- and imidazole-C-H $\cdots$ O(oxido) and  
20 methylene-C-H $\cdots$ O(amide) interactions resulting in a double-layer, Fig. SI 9(a). Alternatively,  
21 the packing can be described as comprising supramolecular layers sustained by the  
22 aforementioned C-H $\cdots$ O interactions, see Fig. SI 9(b), which are clipped into a double-layer by  
23 the N-H $\cdots$ O hydrogen bonds. The double-layers stack along the c-axis direction without  
24 directional interactions between them.

25 In the molecular packing of **3**, analogous imidazole-N-H $\cdots$ O(phenoxide, ethoxy) hydrogen  
26 bonding and five-membered { $\cdots$ H $\cdots$ OC<sub>2</sub>O} synthons are formed as seen for **2** but, in this case,  
27 these extend to form a one-dimensional supramolecular chain as shown in Fig. 5(c). The chain  
28 is orientated along the a-axis and has a helical topology, being propagated by screw (2<sub>1</sub>)  
29 symmetry; additional stability to the chain is provided by imidazole-C-H $\cdots$ O(oxido)

1 interactions. Chains are connected laterally to form a supramolecular layer in the ab-plane via  
2 phenyl-C–H $\cdots$ O(oxido) contacts, see Fig. SI 10(a). The most prominent points of contact  
3 between layers along the c-axis direction are S $\cdots$ O secondary bonding interactions (S1 $\cdots$ O2<sup>i</sup> =  
4 3.068(2) Å for (i): 1-x, ½+y, ½-z). Such interactions are well-known but, are gaining  
5 increasing recognition for their importance in stabilising molecular packing [91-93]; a view of  
6 the unit cell contents is shown in Fig. SI 10(b).

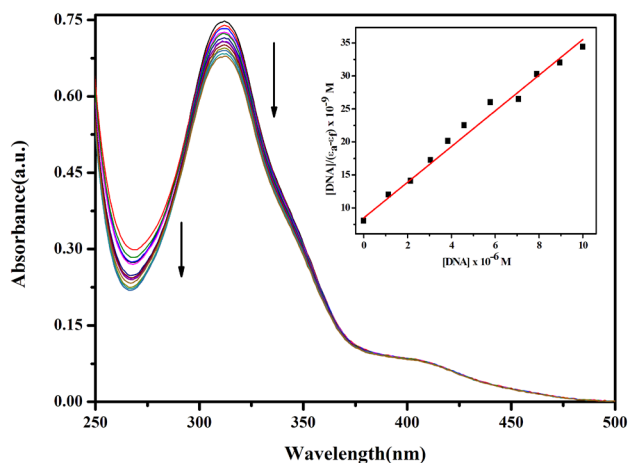
7 The inclusion of a water molecule, albeit statistically disordered about a centre of inversion,  
8 provides the cohesion to the molecular packing in the crystal of **4**. The imidazole-N–H forms  
9 hydrogen bonds to each of the disordered water-O atoms, with the water-O–H donor atoms  
10 forming hydrogen bonds to oxido-O and pyridyl-N atoms. In this way, six molecules of **4** are  
11 assembled about the water molecule. As there are peripheral oxido, imidazole and pyridyl  
12 residues in the seven-molecule aggregate, a three-dimensional architecture is generated as  
13 illustrated in Fig. SI 11.

## 1 DNA Binding Studies

### 2 Absorption spectroscopic studies

3 Applying spectral techniques, the DNA binding affinity of the complexes **1–4** to CT-DNA was  
4 studied and the equilibrium binding constant ( $K_b$ ) of the complexes to CT-DNA was established  
5 (Table 4 and Fig. 6). Complexes **1–4** exhibit absorption bands in the regions 450–400, 340–300  
6 that are attributed to L–Mo( $d\pi$ ) and LMCT transitions while bands at 260–290 nm are due to  
7 intraligand transitions [76]. On adding CT-DNA, complex **1** showed a hyperchromic shift in the  
8 L–Mo( $d\pi$ ) LMCT region whereas hypochromic shifts were observed in both the 340–300 and 260–  
9 290 nm ranges; Fig. SI 12(a). For **2–4**, hypochromic shifts were found in all three ranges; Fig. 6  
10 and Figs SI 12(b)–(c). Both the hyperchromic and hypochromic shifts indicate the interaction of  
11 the CT-DNA with the dioxidomolybdenum complexes. The hyper chromic shift observed may be  
12 either due to electrostatic binding of the complexes to the DNA i.e. the external contact or to the  
13 major and minor grooves of DNA [94,95]. The observed hypochromic shifts may be due to the  
14 interaction between the electronic states of ligand chromophores and the DNA bases [96-98]. The  
15 hypochromism or hyperchromism observed in these cases were used to estimate the binding  
16 strength of the complexes to the CT-DNA. For all complexes, the 260–290 nm range showed a  
17 significant hypochromism which may be due to the higher binding affinity towards CT-DNA in  
18 the lower wavelength region. The equilibrium binding constant ( $K_b$ ) between CT-DNA and each  
19 of the complexes **1–4** was calculated using Eqn 1 (given above).

20 The  $K_b$  values are shown in Table 4 and revealed that **4** has the highest binding affinity of  $3.57 \times$   
21  $10^4 \text{ M}^{-1}$  and **1** has the lowest binding affinity of  $9.91 \times 10^3 \text{ M}^{-1}$ . All complexes display moderate  
22 binding affinity, and the DNA binding strength of the complexes are in the order of **4 > 3 > 2 > 1**  
23 (Table 4). There were no significant interactions observed for the ligands towards CT-DNA.



1  
 2 **Fig. 6.** Electronic absorption spectra of  $[\text{Mo}^{\text{VI}}\text{O}_2\text{L}^4(\text{Q})]_2\cdot\text{H}_2\text{O}$  (**4**) ( $25\ \mu\text{M}$ ) upon the titration of  
 3 CT-DNA ( $0\text{--}110\ \mu\text{M}$ ) in  $50\ \text{mM}$  Tris-HCl buffer ( $\text{pH}\ 8.0$ ). The arrow indicates the changes in  
 4 absorbance intensity with respect to an increase in the concentration of CT-DNA. The inset shows  
 5 the linear fit of  $[\text{DNA}]/(\epsilon_a - \epsilon_f)$  vs.  $[\text{DNA}]$ .

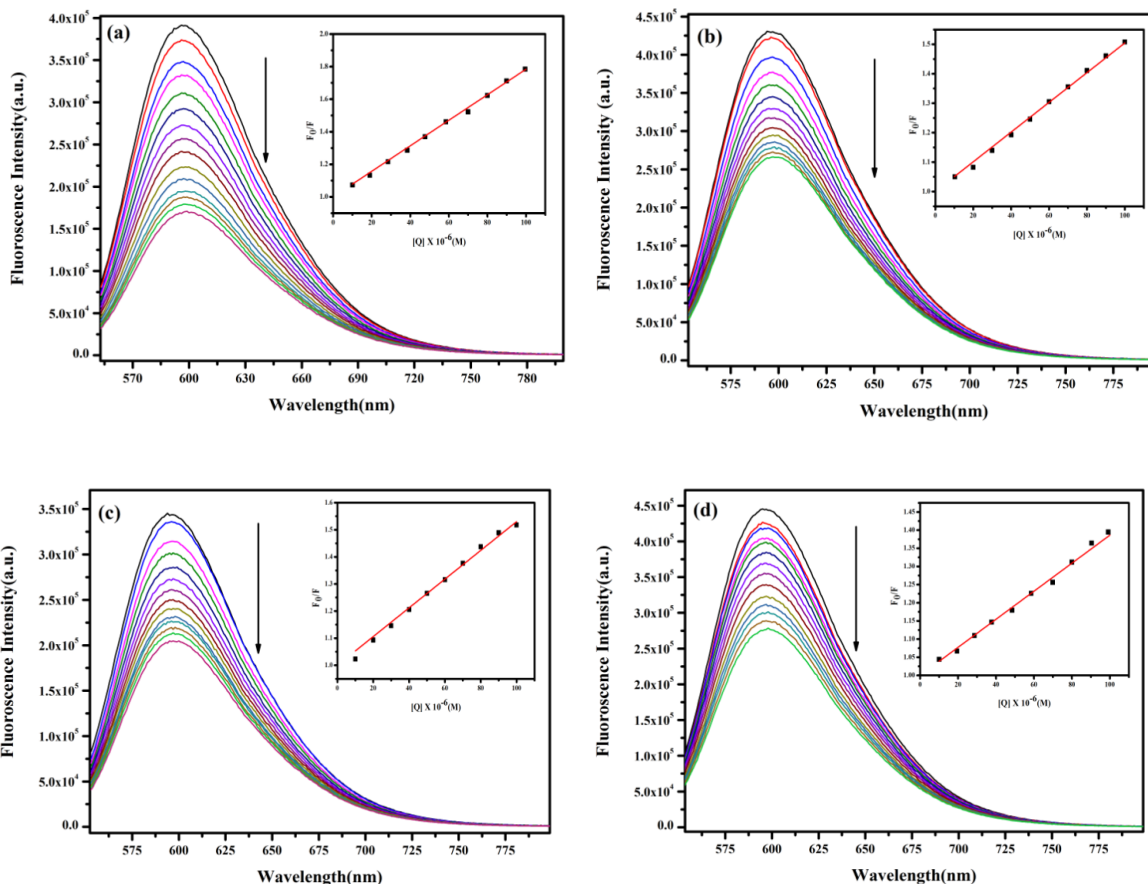
6 **Table 4.** CT-DNA Binding parameters for complexes **1-4**.

Complex	Binding Constant ( $K_b$ ) ( $\text{M}^{-1}$ )	Bimolecular rate constant ( $K_q$ ) Value( $\text{M}^{-1}\text{s}^{-1}$ )
<b>1</b>	$9.91 \times 10^3$	$6.25 \times 10^{11}$
<b>2</b>	$1.49 \times 10^4$	$8.16 \times 10^{11}$
<b>3</b>	$2.61 \times 10^4$	$8.58 \times 10^{11}$
<b>4</b>	$3.57 \times 10^4$	$1.27 \times 10^{12}$

7  
 8  
 9  
 10

## 1 **Competitive Binding Studies**

2 In an attempt to determine the exact mode of binding of the complexes to CT-DNA, competitive  
3 binding experiments were performed with three fluorescent dyes namely 4',6-diamidino-2-  
4 phenylindole (DAPI), methyl green (MG) and ethidium bromide (EB). Among the three, EB tends  
5 to bind DNA through an intercalation mode whereas DAPI and MG bind the minor and major  
6 grooves, respectively [71]. Titration of EB with increasing concentration of complex show the  
7 quenching of emission intensity of EB bound to CT-DNA at 596 nm with a bathochromic shift.  
8 Thus, the indicated displacement of CT-DNA bound EB by **1-4** shows the binding through  
9 intercalation mode; Fig. 7 and Fig. SI 13. The bimolecular rate constant ( $K_q$ ) of EB quenching was  
10 determined by following the Stern–Volmer equation and was found to be in the range  $6.25 \times 10^{11}$   
11  $- 1.27 \times 10^{12} \text{ M}^{-1} \text{ s}^{-1}$  (Table 4). Further, on titration of DAPI bound CT-DNA with increasing  
12 concentration of the complexes, **1** and **3** showed the quenching of emission intensity at 451 nm  
13 with a visible hypsochromic shift, whereas **2** shows a bathochromic shift at the same range in the  
14 emission maxima (Fig. SI 14). From the data it also shows that except for **4**, **1-3** bind to CT-DNA  
15 through minor groove binding mode. All complexes exhibited the quenching of  $\sim 53\%$  for **1**  
16 followed by  $\sim 56\%$  and  $\sim 62\%$  for **2** and **3**, respectively at the fluorescence intensity of 451 nm.  
17 On the other hand, only for complex **4** was a proportionate binding observed on titration with MG  
18 bound CT-DNA. A bathochromic shift is observed at 663 nm, confirming the major groove  
19 binding mode of **4** to CT-DNA (Fig. SI 15). Hence, these data prove that **1-3** along with an  
20 intercalative mode of binding also bind to CT-DNA through minor groove binding, while **4** binds  
21 through intercalation and in the major groove binding mode.



1

2

3 **Fig. 7.** Fluorescence quenching of EB (10 μM) upon the titration of complex **1** (a), **2** (b), **3** (c) and  
 4 **4** (d) (0–100 μM each). The arrows indicate the decrease in fluorescence intensity with respect to  
 5 an increase in the complex concentration; the inset shows the Stern-Volmer plot of the respective  
 6 complexes.

7 ***In vitro* cytotoxic activity**

8 **MTT assay**

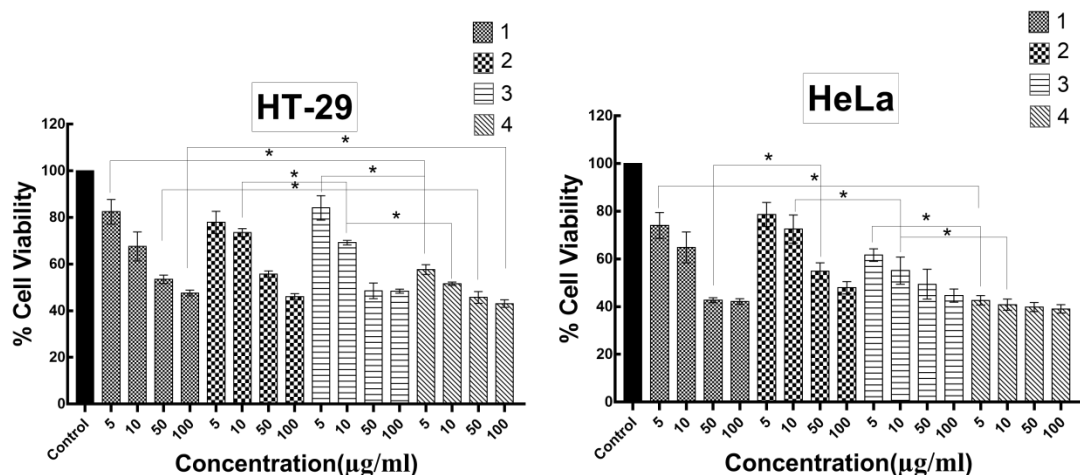
9 In order to understand the *in vitro* cytotoxic potential of the synthesized complexes, an MTT assay  
 10 was performed against two cancer cell lines HT-29 and HeLa after 48 h of incubation. As the test  
 11 complexes were dissolved in DMSO, DMSO was taken as a control experiment so as to identify  
 12 the role of solvent in cytotoxicity of the complexes. The results obtained were analyzed through a

1 % cell viability profile and expressed in terms of their IC<sub>50</sub> values, as depicted in Fig. 8 and Table  
2 5. The aroylhydrazone ligands gave high IC<sub>50</sub> values of > 300 μM. Among all the complexes, **4**  
3 proved to be the most active against both the cell lines. It was capable of killing almost 50% of the  
4 cell population even at a concentration of 5μg/ml. While the rest of the complexes proved to be  
5 less potent.

6 Lately, remarkable cytotoxic activities have been reported for molybdenum complexes against  
7 various human cancer cell lines such as A-549(lung cancer), HeLa (cervical carcinoma) and MCF-  
8 7 (breast carcinoma) [99-103]. Cytotoxicity of **4** was found to be comparable and even better than  
9 those of some clinical drugs and various previous reports of molybdenum complexes as cytotoxic  
10 agents [104-107]. After analysing both DNA binding and cytotoxicity result it was observed that  
11 among the four complexes, mixed ligand complexes **2–4** showed better biological activity than  
12 that of complex **1**, with a coordinated methanol molecule. While complex **4** showed the highest  
13 cytotoxicity among the three mixed ligand complexes, probably due to the presence of heterocyclic  
14 2-hydroxy-1-naphthyl functional group attached to the ligand backbone in comparison to **2** and **3**  
15 [32,34,108].

16

17



1  
2 **Fig. 8.** Cell viability profile of 1-4 against HT-29 and HeLa after 48h of incubation. Data are  
3 reported as the mean  $\pm$  SD for  $n = 4$  and  $*p < 0.05$  statistical differences between treatment of  
4 complexes 1–4.

5 **Table 5.** IC<sub>50</sub> values of 1-4.

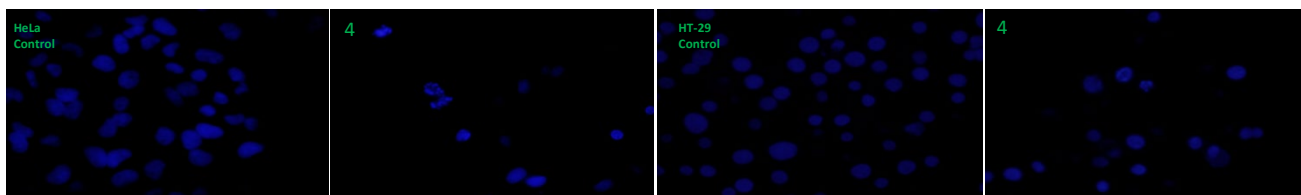
Complexes	IC <sub>50</sub> (µM)	IC <sub>50</sub> (µM)
	HT-29	HeLa
<b>1</b>	177.92 $\pm$ 5.41	84.63 $\pm$ 3.26
<b>2</b>	150.89 $\pm$ 2.65	162.55 $\pm$ 1.54
<b>3</b>	96.26 $\pm$ 0.80	60.64 $\pm$ 3.81
<b>4</b>	20.63 $\pm$ 0.71	4.41 $\pm$ 0.98

6 **DAPI Staining**

7 As complex 4 proved to be the most potent among the series, it was logical to study its effect on  
8 the nuclear morphology of both cancer cell lines. This was studied through DAPI staining. Cells  
9 were treated at a concentration of 50 µg/ml of 4 for a period of 24 h, after which they were stained  
10 with DAPI and examined under a fluorescence microscope. From the images (Fig. 9) it could be  
11 deduced that there were condensed chromatin bodies, nuclear blebbings and shrunken morphology



1 in the cells treated with **4**, whereas there were hardly any condensation observed in the control  
2 image. These phenomena are indicative of apoptosis taking place as the mechanism of cell death  
3 in response to treatment with **4**.



4 **Fig. 9.** Morphology of HeLa and HT-29 control and cells treated with complex **4** for 24 h. The  
5 cells were stained with DAPI and visualized under fluorescent microscope. Scale bar corresponds  
6 to 20  $\mu\text{m}$ .

## 7 **Conclusions**

8 In summary, this article presents the synthesis and characterization of four new mixed ligand  
9 dioxidomolybdenum(VI)  $[\text{Mo}^{\text{VI}}\text{O}_2\text{L}^{1-3}(\text{Q})]$  (**1–3**) and  $[\text{Mo}^{\text{VI}}\text{O}_2\text{L}^4(\text{Q})]_2\cdot\text{H}_2\text{O}$  (**4**) [where Q = MeOH  
10 for **1** and imidazole for **2–4**] complexes from tridentate arolyazine ligand systems ( $\text{H}_2\text{L}^{1-4}$ ). Single  
11 crystal X-ray crystallography revealed a distorted octahedral structure in each case. Hydrogen  
12 bonding features in the molecular packing of **1–4**, lead to supramolecular dimeric aggregates in **1**  
13 and **2**, a helical chain in **3** and a three-dimensional architecture in **4**.

14 The present series of complexes were tested for biological properties in terms of their DNA binding  
15 ability and *in vitro* cytotoxicity. The study revealed that the complexes bind moderately with CT-  
16 DNA via intercalative, minor and major groove modes, while **4** showed the highest binding affinity  
17 compared to the other complexes. Also, the result of an antiproliferative study revealed **4** to be the  
18 most cytotoxic towards both HT-29 and HeLa cancer cell lines among the series. The presence of

1 imidazole as a co-ligand along with a heterocyclic 2-hydroxy-1-naphthyl moiety in the ligand  
2 backbone of **4** may be responsible for a better interaction with DNA as well as cytotoxicity in  
3 comparison to the other complexes. The outcome of the present study will definitely boost further  
4 research on the design of dioxidomolybdenum complexes as metal-based agents for anticancer  
5 studies.

#### 6 **Appendix A. Supplementary material**

7 Crystallographic data for **1-4** reported in this paper have been deposited with the Cambridge  
8 Crystallographic Data Centre (CCDC) as supplementary publication nos 1920543-1920546 for **1-**  
9 **4**, respectively. These data can be obtained free of charge via [www.ccdc.cam.ac.uk/getstructures](http://www.ccdc.cam.ac.uk/getstructures).  
10 Geometric data characterising the chelate rings are given in Table SI 1 and crystallographic  
11 diagrams and details of the specified intermolecular interactions are given in Figs SI 7-11 whereas  
12 the spectra are given in Figs SI 1-6 and SI 12-15.

#### 13 **Acknowledgements**

14 R. D thanks DBT, Govt. of India [Grant No. 6242-P112/RGCB/ PMD/DBT/RPDA/2015] and  
15 CSIR, Govt. of India [Grant No. 01(2963)/18/EMR-II] for funding this research. The authors also  
16 thank Sunway University Sdn Bhd (Grant no. STR-RCTR-RCCM-001-2019) for support of  
17 crystallographic studies.

18

## 1 References

- 2 1. C. Beedham, Molybdenum hydroxylases as drug-metabolizing enzymes, *Drug Metab Rev*  
3 16 (1985) 119–156.
- 4 2. R.C. Bray, *Quart. Rev. Biophys.* 21 (1988) 299–329.
- 5 3. J.P.G. Malthouse, R.C. Bray, *Biochem. J.* 191 (1980) 265–267.
- 6 4. R.H. Holm, *Chem. Rev.* 87 (1987) 1401–1449.
- 7 5. Y.-L. Qiao, S.M. Dawsey, F. Kamangar, J.-H. Fan, C.C. Abnet, X.-D. Sun, L.L. Johnson,  
8 M.H. Gail, Z.-W. Dong, B. Yu, S.D. Mark, P.R. Taylor, *J. Natl. Cancer Inst.* 101 (2009)  
9 507–518.
- 10 6. J. Honziček, J. Vinklárek, M. Erben, Z. Padělková, L. Šebestová, M. Řezáčová, J.  
11 *Organomet. Chem.* 749 (2014) 387–393.
- 12 7. M.R.P. Norton de Matos, C.C. Romão, C.C.L. Pereira, S.S. Rodrigues, M. Mora, M.J.P.  
13 Silva, P.M. Alves, C.A. Reis, *International Patent WO/2005/087783*.
- 14 8. J. Feng, X. Lu, G. Wang, S. Du, Y. Cheng, *Dalton Trans.* 41 (2012) 8697–8702.
- 15 9. A.K. Sah, N. Baig, *Catal. Lett.* 145 (2015) 905–909.
- 16 10. Z. Hu, X. Fu, Y. Li *Inorg. Chem. Commun.* 14 (2011) 497–507.
- 17 11. S. N. Rao, N. Kathale, N. N. Rao, K. N. Munshi, *Inorg. Chim. Acta* 360 (2007) 4010–4016.
- 18 12. Y. Li, X. Fu, B. Gong, X. Zou, X. Tu, J. Chen, *J. Mol. Catal. A: Chem.* 322 (2010) 55–62.
- 19 13. M. Masteri-Farahani, F. Farzaneh, M. Ghandi, *J. Mol. Catal. A: Chem.* 248 (2006) 53–60.
- 20 14. M. Masteri-Farahani, F. Farzaneh, M. Ghandi, *Catal. Commun.* 8 (2007) 6–10.
- 21 15. A. Rezaeifard, I. Sheikhshoae, N. Monadi, M. Alipour, *Polyhedron* 29 (2010) 2703–2709.
- 22 16. F.E. Kuhn, A.M. Santos, A.D. Lopes, I.S. Goncalves, J. E. Rodri'guez-Borges, M.  
23 Pillinger, C.C. Romão, *J. Organomet. Chem.* 621 (2001) 207–217.

- 1 17. M. Groarke, I.S. Goncalves, W.A. Herrmann, F.E. Kuhn, *J. Organomet. Chem.* 649 (2002)  
2 108–112.
- 3 18. J. Fridgen, W.A. Herrmann, G. Eickerling, A.M. Santos, F.E. Kuhn, *J. Organomet. Chem.*  
4 689 (2004) 2752–2761.
- 5 19. A. Sakthivel, J. Zhao, G. Raudaschl-Sieber, M. Hanzlik, A.S.T. Chiang, F.E. Kuhn, *Appl.*  
6 *Catal. A: Gen.* 281 (2005) 267–273.
- 7 20. I.S. Goncalves, A.M. Santos, C.C. Romao, A.D. Lopes, J.E. Rodri'guez-Borges, M.  
8 Pillinger, P. Ferreira, J. Rocha, F.E. Kuhn, *J. Mol. Catal. A: Chem.* 222 (2004) 265–271.
- 9 21. S. P. Dash, S. Majumder, A. Banerjee, M. F. N. N. Carvalho, P. Adão, J. Costa Pessoa, K.  
10 Brzezinski, E. Garribba, H. Reuter, R. Dinda, *Inorg. Chem.* 55 (2016) 1165–1182.
- 11 22. S. P. Dash, S. Roy, M. Mohanty, M. F. N. N. Carvalho, M. L. Kuznetsov, J. C. Pessoa, A.  
12 Kumar, Y. P. Patil, A. Crochet, R. Dinda, *Inorg. Chem.* 55 (2016) 8407–8421.
- 13 23. M. Mancka, W. Plass, *Inorg. Chem. Commun.* 10 (2007) 677–680.
- 14 24. S. P. Dash, S. Pasayat, S. Bhakat, S. Roy, R. Dinda, E. R. T. Tiekink, S. Mukhopadhyay,  
15 S. K. Bhutia, M. R. Hardikar, B. N. Joshi, Y. P. Patil, M. Nethaji, *Inorg. Chem.* 52 (2013)  
16 14096–14107.
- 17 25. S. Naskar, M. Corbella, A. J. Blake, S. K. Chattopadhyay, *Dalton Trans.* (2007) 1150–  
18 1159.
- 19 26. D. S. Raja, N. S. P. Bhuvanesh, K. Natarajan, *J. Biol. Inorg. Chem.* 17 (2012) 223–237.
- 20 27. T. B. Chaston, D. R. Richardson, *J. Biol. Inorg. Chem.* 8 (2003) 427–438.
- 21 28. Q. Wang, Z. Y. Yang, G. F. Qi, D. D. Qin, *Biometals* 22 (2009) 927–940.
- 22 29. Z. Y. Yang, B. D. Wang, Y. H. Li, *J. Organomet. Chem.* 691 (2006) 4159–4166.

- 1 30. B. D. Wang, Z. Y. Yang, P. Crewdson, D. Q. Wang, J. Inorg. Biochem. 101 (2007) 1492–  
2 1504.
- 3 31. T. R. Li, Z. Y. Yang, B. D. Wang, D. D. Qin, Eur. J. Med. Chem. 43 (2008) 1688–1695.
- 4 32. Q. Wang, Z. Y. Yang, G. F. Qi, D. D. Qin, Eur. J. Med. Chem. 44 (2009) 2425–2433.
- 5 33. Z. C. Liu, B. D. Wang, Z. Y. Yang, Y. Li, D. D. Qin, T. R. Li, Eur. J. Med. Chem. 44  
6 (2009) 4477–4484.
- 7 34. Y. Li, Z. Y. Yang, M. F. Wang, Eur. J. Med. Chem. 44 (2009) 4585–4595.
- 8 35. K. Ghosh, P. Kumar, N. Tyagi, U. P. Singh, V. Aggarwal, M. C. Baratto, Eur. J. Med.  
9 Chem. 45 (2010) 3770–3779.
- 10 36. Z. C. Liu, B. D. Wang, B. Li, Q. Wang, Z. Y. Yang, T. R. Li, Y. Li, Eur. J. Med. Chem.  
11 45 (2010) 5353–5361.
- 12 37. P. Krishnamoorthy, P. Sathyadevi, A. H. Cowley, R. R. Butorac, N. Dharmaraj, Eur. J.  
13 Med. Chem. 46 (2011) 3376–3387.
- 14 38. B. D. Wang, Z. Y. Yang, T. R. Li, Bioorg. Med. Chem. 14 (2006) 6012–6021.
- 15 39. P. Krishnamoorthy, P. Sathyadevi, R. R. Butorac, A. H. Cowley, N. S. P. Bhuvanesh, N.  
16 Dharmaraj, Dalton Trans. 41 (2012) 4423–4436.
- 17 40. M. Alagesan, N. S. P. Bhuvanesh, N. Dharmaraj, Dalton Trans. 42 (2013) 7210–7223.
- 18 41. A. C. Cunha, J. M. Figueiredo, J. L. M. Tributino, A. L. P. Miranda, H. C. Castro, R. B.  
19 Zingali, C. A. M. Fraga, M. C. B. V. Souza, V. F. Ferreira, E. Barreiro, J. Bioorg. Med.  
20 Chem. 11 (2003) 2051–2059
- 21 42. J. Easmon, G. Puerstinger, K. S. Thies, G. Heinisch, J. Hofmann, J. Med. Chem. 49 (2006)  
22 6343–6350.

- 1 43. T. B. Chaston, R. N. Watts, J. Yuan, D. R. Richardson, *Clin. Cancer Res.* 10 (2004) 7365–  
2 7374.
- 3 44. V. Singh, V. K. Srivastava, G. Palit, K. Shankar, A. – *Forsch, Drug. Res.* 42 (1992) 993–  
4 996.
- 5 45. N. Singh, R. Ranjana, M. Kumari, B. Kumar, *IJPCR* 8 (2016) 162–166.
- 6 46. A. G. Tempone, R. A. Mortara, H. F. De Andrade Jr., J. Q. Reimão, *Int. J. Antimicrob.*  
7 *Agents*, 36 (2010) 159–163.
- 8 47. F. Léonard, A. Andrémont, C. Tancrede, *J. Appl. Bacteriol.* 58 (1985) 545–553.
- 9 48. S. Patterson, S. Wyllie, *Trends Parasitol.*, 30 (2014) 289–298.
- 10 49. L. J. Rubin, R. H. Peter, *J. Med.* 302 (1980) 69–73.
- 11 50. S. Todorovic, N. Juranic, S. Macura, F. Rusnak, *J. Am. Chem. Soc.* 121 (1999) 10962–  
12 10966.
- 13 51. O. Pouralimardan, A. Chamayou, C. Janiak, H. Monfared, *Inorg Chim Acta* 360 (2007)  
14 1599–1608.
- 15 52. C. Basu, S. Chowdhury, R. Banerjee, H. S. Evans, S. Mukherjee, *Polyhedron* 26 (2007)  
16 3617–3624.
- 17 53. M. Bakir, O. Green, W. H. Mulder, *J Mol Struct.* 873 (2008) 17–28.
- 18 54. P. Melnyk, V. Leroux, C. Sergheraert, P. Grellier, *Bioorg. Med. Chem. Lett.* 16 (2006)  
19 31–35.
- 20 55. S. G. Kucukguzel, A. Mazi, F. Sahin, S. Ozturk, J. Stables. *Eur. J. Med. Chem.* 38 (2003)  
21 1005-1013.
- 22 56. D. Sriram, P. Yoggeswari, K. Madhu, *Bioorg. Med. Chem. Lett.* 15 (2005) 4502–4505.

- 1 57. S. G. Kucukguzel, S. Rollas, I. Kucukguzel, M. Kiraz, *Eur. J. Med. Chem.* 34 (1999) 1093–  
2 1100.
- 3 58. S. Gemma, G. Kukreja, C. Fattorusso, M. Persico, M. P. Romano, M. Altarelli, L. Savini,  
4 G. Campiani, E. Fattorusso, N. Basilico, D. Taramelli, V. Yardley, S. Butini. *Bioorg. Med.*  
5 *Chem. Lett.* 16 (2006) 5384–5388.
- 6 59. F. Bellina, S. Cauteruccio, R. Rossi, *Tetrahedron* 63(2007) 4571–4624.
- 7 60. R. Di Santo, A. Tafi, R. Costi, M. Botta, M. Artico, F. Corelli, M. Forte, F. Caporuscio, L.  
8 Angiolella, A. T. Palamara, *J. Med. Chem.* 48 (2005) 5140–5153.
- 9 61. S. Dutta, *Acta Pharmaceutica* 60 (2010) 229–235.
- 10 62. A. Banerjee, S. P. Dash, M. Mohanty, D. Sanna, G. Sciortino, V. Ugone, E. Garribba, H.  
11 Reuter, W. Kaminsky, R. Dinda, *J. Inorg. Biochem.* 199 (2019) 110786.
- 12 63. M. Mohanty, S. K. Maurya, A. Banerjee, S. A. Patra, M. R. Maurya, A. Crochet, K.  
13 Brzezinski, R. Dinda, *New J. Chem.* (2019) 10.1039/c9nj01815h
- 14 64. S. Lima, A. Banerjee, M. Mohanty, G. Sahu, C. Kausar, S. K. Patra, E. Garribba, W.  
15 Kaminsky, R. Dinda, *New J. Chem.* (2019) 10.1039/c9nj01910c
- 16 65. S. Majumder, S. Pasayat, S. Roy, S. P. Dash, S. Dhaka, M. R. Maurya, M. Reichelt, H.  
17 Reuter, K. Brzezinski, R. Dinda, *Inorg. Chim. Acta* 469 (2018) 366–378.
- 18 66. S. Majumder, S. Pasayat, A. K. Panda, S. P. Dash, S. Roy, A. Biswas, M. E. Varma, B. N.  
19 Joshi, E. Garribba, C. Kausar, S. K. Patra, W. Kaminsky, A. Crochet, R. Dinda, *Inorg.*  
20 *Chem.* 56 (2017) 11190–11210.
- 21 67. S. P. Dash, A. K. Panda, S. Dhaka, S. Pasayat, A. Biswas, M. R. Maurya, P. K. Majhi, A.  
22 Crochet, R. Dinda, *Dalton Trans.* 45 (2016) 18292–18307.

- 1 68. S. Pasayat, M. Böhme, S. Dhaka, S. P. Dash, S. Majumder, M. R. Maurya, W. Plass, W.  
2 Kaminsky, R. Dinda, *Eur. J. Inorg. Chem.* 10 (2016) 1604–1618.
- 3 69. Saswati, A. Chakraborty, S. P. Dash, A. K. Panda, R. Acharyya, A. Biswas, S.  
4 Mukhopadhyay, S. K. Bhutia, A. Crochet, Y. P. Patil, M. Nethaji, R. Dinda, *Dalton Trans.*  
5 44 (2015) 6140–6157.
- 6 70. S. P. Dash, A. K. Panda, S. Pasayat, S. Majumder, A. Biswas, W. Kaminsky, S.  
7 Mukhopadhyay, S. K. Bhutia, R. Dinda, *J. Inorg. Biochem.* 144 (2015) 1–12.
- 8 71. S. P. Dash, A. K. Panda, S. Pasayat, R. Dinda, A. Biswas, E. R. T. Tiekink, S.  
9 Mukhopadhyay, S. K. Bhutia, W. Kaminsky, E. Sinn, *RSC Adv.* 5 (2015) 51852–51867.
- 10 72. S. Pasayat, S. P. Dash, S. Majumder, R. Dinda, E. Sinn, H. Stoeckli-Evans, S.  
11 Mukhopadhyay, S. K. Bhutia, P. Mitra, *Polyhedron* 80 (2014) 198–205.
- 12 73. S. P. Dash, A. K. Panda, S. Pasayat, R. Dinda, A. Biswas, E. R. T. Tiekink, Y. P. Patil, M.  
13 Nethaji, W. Kaminsky, S. Mukhopadhyay, S. K. Bhutia, *Dalton Trans.* 43 (2014) 10139–  
14 10156.
- 15 74. S. Pasayat, S. P. Dash, S. Roy, R. Dinda, S. Dhaka, M. R. Maurya, W. Kaminsky, Y. P.  
16 Patil, M. Nethaji, *Polyhedron* 67 (2014) 1–10.
- 17 75. R. Dinda, P. Sengupta, M. Sutradhar, T. C. W. Mak, S. Ghosh, *Inorg. Chem.* 47 (2008)  
18 5634–5641.
- 19 76. R. Dinda, P. Sengupta, S. Ghosh, W. S. Sheldrick, *Eur. J. Inorg. Chem.* 2003 (2003) 363–  
20 369.
- 21 77. R. Dinda, P. Sengupta, S. Ghosh, T. C. W. Mak, *Inorg. Chem.* 41 (2002) 1684–1688.
- 22 78. S. Purohit, A. P. Koley, L. S. Prasad, P. T. Manoharan, S. Ghosh, *Inorg. Chem.* 283 (1989)  
23 735–741.



- 1 79. G. J. -J. Chen, J. W. McDonald, W. E. Newton, *Inorg. Chem.* 15 (1976) 2612–2615.
- 2 80. Rigaku Oxford Diffraction, CrysAlis PRO, Yarnton, Oxfordshire, England, 2017.
- 3 81. Agilent Technologies, CrysAlis PRO, Agilent Technologies, Yarnton, Oxfordshire,  
4 England, 2010
- 5 82. G. M. Sheldrick, *Acta Crystallogr. A* 64 (2008) 112–122.
- 6 83. G. M. Sheldrick, *Acta Crystallogr. C* 71 (2015) 3–8.
- 7 84. L. J. Farrugia, *J. Appl. Crystallogr.* 45 (2012) 849–854.
- 8 85. DIAMOND, Visual Crystal Structure Information System, Version 3.1, CRYSTAL  
9 IMPACT, Postfach 1251, D–53002 Bonn, Germany, (2006).
- 10 86. A. L. Spek, *Acta Crystallogr. Sect. D: Biol. Crystallogr.* 65 (2009) 148–155.
- 11 87. N.-ul H. Khan, N. Pandya, N. C. Maity, M. Kumar, R. M. Patel, R. I. Kureshy, S. H. R.  
12 Abdi, S. Mishra, S. Das, H. C. Bajaj, *Eur. J. Med. Chem.* 46 (2011) 5074–5085.
- 13 88. C. Artner, H. U. Holtkamp, C. G. Hartinger, S. M. M.-Menches, *J. Inorg. Biochem.* 177  
14 (2017) 322–327.
- 15 89. S. Das, G. P. Muthukumaragopal, S. N. Pal, S. Pal, *New J. Chem.* 27 (2003) 1102–1107.
- 16 90. R. Dinda, P. Sengupta, S. Ghosh, H. Mayer-Figge, W. S. Sheldrick *J. Chem. Soc., Dalton*  
17 *Trans.* (2002) 4434–4439
- 18 91. N.W. Alcock, *Adv. Inorg. Chem.* 15 (1972) 1–58.
- 19 92. E.R.T. Tiekink, *Coord. Chem. Rev.* 345 (2017) 209–228.
- 20 93. L. Vogel, P. Woner, S.M. Huber, *Angew. Chem. Int. Ed.* 58 (2019) 1880–1891.
- 21 94. M. Sakthi, A. Ramu, *J. Mol. Struct.* 1149 (2017) 727–735.
- 22 95. I.M. El-Deen, A.F. Shoair, M.A. El-Bindary, *J. Mol. Struct.* 1180 (2019) 420–437.
- 23 96. F. Arjmand, B. Mohani, S. Ahmad, *Eur. J. Med. Chem.* 40 (2005) 1103–1110.

- 1 97. V. Rajendiran, M. Murali, E. Suresh, S. Sinha, K. Somasundaram, M. Palaniandavar,  
2 Dalton Trans. (2008) 148–163.
- 3 98. F. Arjmand, M. Aziz, Eur. J. Med. Chem. 44 (2009) 834–844.
- 4 99. V. Vrdoljak, I. Đilović, M. Rubčić, S. K. Pavelić, M. Kralj, D. M. Čalogović, I.  
5 Piantanida, P. Novak, A. Rožman, M. Cindrić, Eur. J. Med. Chem. 45 (2010) 38–48
- 6 100. M. S. Saraiva, S. Quintal, F. C. M. Portugal, T. A. Lopes, V. Félix, J. M. F. Nogueira,  
7 M. Meireles, M. G. B. Drew, M. J. Calhorda, J. Organomet. Chem. 693 (2008) 3411–3418.
- 8 101. Y. Jin, H. Lee, M. Pyo, M. S. Lah, Dalton Trans. (2005) 797–803.
- 9 102. M. A. Hussein, T. S. Guan, R. A. Haque, M. B. K. Ahamed, A. M. S. A. Majid,  
10 Polyhedron 85 (2015) 93–103.
- 11 103. H. Thomadaki, A. Karaliota, C. Litos, A. Scorilas, J. Med. Chem. 50 (2007) 1316–1321.
- 12 104. A. Lewis, L. Forrester, J. Hayes, C. Wareing, J. Carmichael, A. Harris, M. Mooghen,  
13 C.R. Wolf, Brit. J. Cancer. 60 (1989) 327–331.
- 14 105. K. Takara, T. Sakaeda, T. Yagami, H. Kobayashi, N. Ohmoto, M. Horinouchi, K.  
15 Nishiguchi, K. Okumura, Biol. Pharm. Bull. 25 (2002) 771–778.
- 16 106. L. Reytman, O. Braitbard, E.Y. Tshuva, Dalton Trans. 41 (2012) 5241–5247.
- 17 107. A. Stockert, D. Kinder, M. Christ, K. Amend, A. Aulthouse, Austin J. Pharmacol. Ther.  
18 2 (2014) 6.
- 19 108. D. S. Raja, N. S. P. Bhuvanesh and K. Natarajan, J. Biol. Inorg. Chem. 17 (2012) 223–  
20 237.